令和 4 年度博士学位論文

Boron nitride nanotubes: purification and alignment studies

窒化ホウ素ナノチューブ：精製と配向の研究

奈良先端科学技術大学院大学

物質創成科学研究科

Florencio Delen De los Reyes

Table of Contents

List of Figures and Tables

Chapter 1

Chapter 2

Chapter 3

List of Tables

Abstract

Boron nitride nanotubes (BNNTs) are emerging nanomaterials attractive in various industries like semiconductors, energy storage systems, and aerospace applications because of their exceptional properties. Theoretical and experimental investigations have increased in the last two decades to gain new insights on BNNTs. Their exotic properties are unavailable to their carbon counterpart, carbon nanotubes (CNTs). BNNTs are as strong as CNTs with Young's modulus up to 1.3 TPa, and are more thermally stable in air than CNTs up to 900 ° C. BNNTs exhibit inherent properties such as a piezoelectric function that can produce electrical responses from stretching and high-neutron absorption that can provide protection against harmful radiation sources.

Moreover, the wide band gap of BNNT, ~5.5 eV, makes them electrically insulating yet thermally conductive. Unarguably, compared to CNTs, BNNTs are much less studied and applied rooting from the mass-production issues and limited liquid and solid processing technologies. This thesis explores the design of a system to produce high-quality BNNT dispersion, translated into highly organized nanostructures.

The successful purification of mass-produced BNNTs fabricated via induction plasma torch method is discussed. A non-aromatic polymer, ethyl cellulose (EC), was examined to wrap the BNNTs uniformly and selectively. The wrapping mechanism is supported by the non-covalent functionalization. This allows the isolation of BNNTs from the hexagonal boron nitride and boron oxides impurities via sonication and density-gradient separation in a solution containing EC. Approximately 55 wt.% of BNNT was retained in the colloidal dispersion using benzyl alcohol as solvent. This yield is higher than the dispersion prepared with previously studied conjugated polymer dissolved in chloroform.

Generally, one-dimensional (ID) nanomaterials are randomly oriented when introduced in nanostructures. The hierarchical organization of BNNTs and CNTs to organized assemblies are substantial to attain optimal properties. From the random BNNT films fabricated using EC systems, highly organized BNNT-polymer assemblies were observed when polyvinyl butyral (PVB) was used instead of EC. The alignment quantification of 1D systems using high-resolution scanning electron microscopy (HR-SEM) images run on Matlab is applied in this work. The degree of alignment was enhanced to 78% BNNTs contained in the uniform deposits of the BNNT films.

In the last part of the thesis, I will deliver a summary and perspective scope of the present research. The initial investigation in this research is valuable for attaining the optimum behavior of BNNT-based nanostructures for advanced applications.

Chapter 1

Introduction to Boron Nitride Nanotubes (BNNTs)

Boron nitride nanotubes (BNNTs) are emerging nanomaterials attractive in various industries like semiconductors, energy storage systems, nanomedicines, and aerospace applications because of their exceptional properties[1–4]. The last two decades have increased theoretical and experimental investigations to gain new insights on BNNTs. Their exotic properties are unavailable to their carbon counterpart, carbon nanotubes (CNTs). Unarguably, compared to CNTs, BNNTs are much less studied and applied rooting from the bulk-production issues and limited liquid and solid processing technologies[5]. Therefore, this dissertation explores the design of a system to produce high-quality BNNTs, translated into highly organized nanostructures.

This opening chapter will provide an overview of the structure, properties, and processing techniques leading to possible future applications. The literature background will cover reviews on the available purification and sorting techniques. From there, we will specify our attempts to contribute to unexplored areas by stating the objectives and scope of the study.

1.1 Structure and properties

A boron nitride nanotube can be imagined as a planar hexagonal boron nitride (hBN) rolled into a single layer BN nanotube (**Fig. 1.1**). It has a similar tubular structure to its carbon nanotube (CNT) counterpart in which alternating B and N atoms fully substitute for C atoms. The B—N bonding possesses a partially ionic character compared to C—C bonding in CNT, resulting to a typical multi-walled (mw-) BNNT system due to the B—N stacking characteristics[6]. In contrast, the weaker van der Waals interaction in CNT makes the formation of a

single-walled (sw-) tubular structure much easier. Transmission electron microscope (TEM) images show various BNNTs with N-number of walls (**Fig. 1.2**). The interwall distance of the mw-BNNT is 3.4 Å. Previously synthesized BNNTs have a diameter ranging from 2 to 50 nm and lengths up to 5 μm.
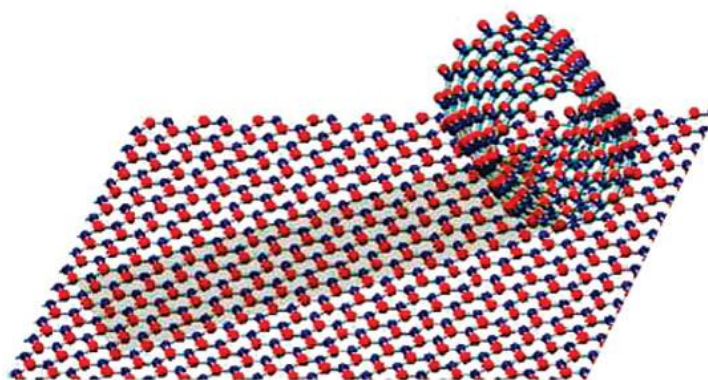
Fig. 1.1 Structural model of BN nanotube rolled from BN. Reproduced from Ref. [6], with permission from American Chemical Society.

The rolling fashion of the planar hBN, indicated by the corresponding (n, m) indices (**Fig. 1.2**) determines the helicity or chirality of BNNT. Armchair (n, n), zigzag (n, 0), and helical (n, m) orientations of BNNTs are synthesized, zigzag configurations being the most common. Previous studies have shown a strong correlation between BNNT walls, each inner wall matching the chirality of the outer shells[7]. Contrastingly, all helicities of CNTs are statistically equal, in which the chirality of the walls are generally random in mw-CNTs[6].

BNNT has excellent mechanical properties and high thermal conductivity[8,9]. The experimental Young's modulus was measured up to TPa level, similar to CNTs[10-12]. The ionic character of the B—N bond remarkably gives

BNNT their inherent properties. The charge transfer from B to N atoms increases the gap between the valence and conduction bands, making BNNT a wide gap semiconductor. The band gap energy is reported between 5 – 6 eV[8,13]. Early theoretical studies found all BNNT structures as semiconducting materials with band gap higher than 2 eV[14]. Narrow BNNT with diameter <1 nm has calculated band gap <2 eV, no experimental studies have produced very small diameter tube. Increasing the diameter up to about 50 nm increases the band gap up to a limit similar to the hBN, ~6 eV . This wide band gap is not dependent to the change in chirality[15].
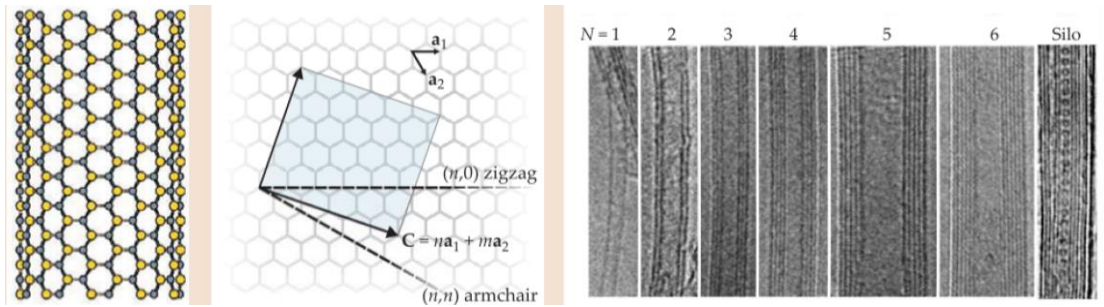
Fig. 1.2 Chirality, n-wall BNNTs. Reproduced from Ref. [16], from Physics Today

The polarized B=N double bond of BNNT also makes them piezoeletric, inducing charge difference from applied mechanical forces[17,18]. Self-assembled BNNT thin films produced a piezoelectric coefficient of 41.12 pm/V higher than commercially available piezoelectrics zinc oxide nanomaterial (12.4 pm/V) and polyvinylidene fluoride (20-28 pm/V)[19]. Molecular dynamics studies have shown the piezoelectric property of mw-BNNTs (**Fig. 1.3**)[20]. For an odd-layer number of wall, piezoelectric polarization increases linearly with increasing radius but decreases with number of layers. On the other hand, for an even-layer number of

wall, the piezoelectric polarization is independent of the radius but increases linearly with number of layers[21].
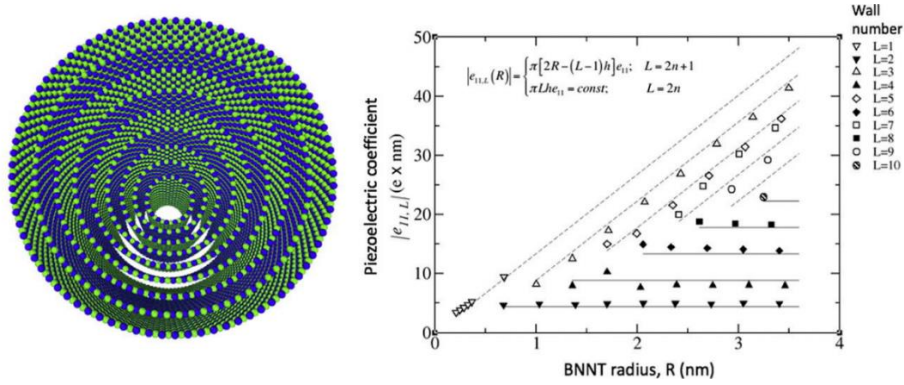
Fig. 1.3 Piezoelectric coefficient of multiwalled-BNNTs. Reproduced from Ref. [21], with permission from Elsevier.

Boron-based compounds like BNNT show high neutron absorption characteristics. Natural boron shows thermal neutron absorption about 760 barns higher than ^{235}U (549 barns) and lower than ^6Li (940 barns)[22]. This makes them one of the best candidates for neutron shielding. The reactions capturing neutron is shown below (**Fig. 1.4**), summarized by equations 1.1 and 1.2. The ^{10}B nucleus transforms to a meta-stable ^{11}B nucleus after capturing a neutron that instantly decays to Li and He atoms.
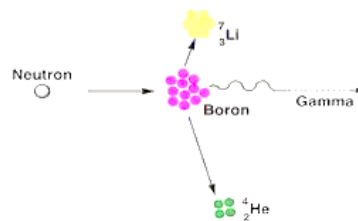
Fig. 1.4 Neutron capture mechanism using Boron

1.2 Methods of synthesis

The theoretical prediction of boron nitride nanotubes in 1994 by Cohen and its first successful synthesis in 1995 by Zettl's[23] lead to considerable growth of research on BNNT. Different methods of synthesis have been done to fabricate BNNTs. The temperature, catalyst, B and N source on these methods have affected their quality and quantity. The most common methods are presented below.

1.2.1 Arc-discharge method

The first BNNT was fabricated by arc-discharge between a BN-packed filament rod and cooled copper electrode[23]. The anode part was quickly vaporized when the arc plasma was generated between the cathode and anode. The fabricated BNNTs had a length of 200 nm and an inner diameter of 1–3 nm. The arc cone occupies a small volume where BNNTs are formed, therefore, only small amounts of BNNTs are produced with this method.

1.2.2 Ball-milling method

The boron powder was ball-milled with ammonia (NH_3) gas followed by annealing in N_2 atmosphere[24]. Long milling time promotes the nitration process between boron and NH_3, giving a higher yield. The optimal annealing temperature was also recorded at1200 ^0C to obtain more BNNT

products. However, promising for low-cost industrial production of BNNTs, the final product contains a considerable number of impurities such as amorphous boron and boron nitride flakes along with BNNT.

1.2.3 Chemical vapor deposition method

The first attempt to synthesize BNNT using chemical vapor deposition (CVD) method was carried out using borazine and metal catalyst like Co and Ni at 100-1100 ^{0}C temperature[25]. CVD was adopted to fabricate BNNT based on carbon nanomaterials method of synthesis. Compared to other methods, it offers better controllability of various parameters like precursors, catalyst, and experimental setup to obtain high-quality nanomaterials[26]. Instead of using gas precursors of B, solid or liquid boron sources are used along with N sources like N_2 or NH_3. The diameter of BNNT produced via CVD method ranges from few nanometers to 70 nm, with length of 10-micrometer. The great control of the experimental conditions also leads to higher quality of BNNT, however, the yield is still considerably low.

1.2.4 Laser-ablation method

The first successful fabrication of BNNT using laser-ablation method was done by Golberg[27]. Multi-walled BNNTs were synthesized using cubic and hexagonal BN melted by laser up to 5000 K under extremely high pressure of nitrogen gas. In this method, the phase transformation of the solid boron or boron nitride to liquid due to laser heating increases the

reaction between boron and the nitrogen atmosphere resulting in more efficient growth of BNNT. The method has produced fewer walls of BNNT of high crystallinity. Gram-scale synthesis has been achieved under high temperature/pressure conditions using boron metal fibers and nitrogen gas by LASA Langley Research center.

1.2.5 Plasma processes

The previously presented methods of synthesis have achieved a gram scale synthesis of higher quality of BNNTs. The milligram per hour rate via laser-ablation method, however, is still limited due to the restraint on the area where BNNT can grow. Hence, alternative methods using plasma have been done[28,29] where higher thermal energy can be distributed over a larger volume making it possible to produce more BNNTs.

Thermal plasma jet method is done using two concentric electrodes, the anode, and the cathode. The arc plasma jet is formed when gas mixtures containing Ar, N_2, and H_2 flow between the electrodes[30]. A high production rate of 20 grams per hour BNNTs was achieved using Radio Frequency induction plasma jet process[31]. The highly crystalline and few-walled BNNT formed has a diameter of 5 nm.

1.3 Purification, dispersion, and functionalization

The trade-off in the quantity and quality of BNNT produced by existing fabrication methods has limited large-amount application of high-quality BNNT. Recent advances in producing gram-scale of BNNT via high temperature and pressure (HTP) laser ablation techniques and plasma processes greatly improved the BNNT quality, however, significant number of impurities containing boron and its oxides, and different forms of boron nitride, most distinguishably hexagonal boron nitride (h-BN), are also formed[32,33]. The impurities affect the dispersibility, solubility, and stability of BNNT in solution[34]. They alter the properties of BNNT for various practical applications. The mechanical strength and thermal conductivity are sub-optimal when BNNTs are used as reinforcement in nanocomposites.

1.3.1 Removal of elemental boron and its oxides

The removal of elemental boron and its oxides are well established[35]. The presence of amorphous boron makes the bulk-produced BNNTs gray in comparison to white to yellowish form of oxidized BNNT (**Fig. 1.5**).
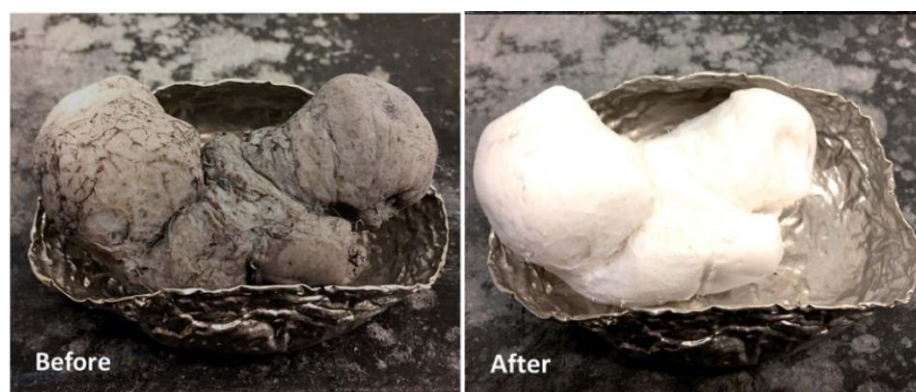
Fig. 1.5 Bulk-produced BNNT before and after oxidation. Reproduced from Ref. [32] with permissions from Nanoscale Advances and RSC.

The raw materials are oxidized in air to convert amorphous boron to their oxide form. The thermogram profile (**Fig. 1.6**) of BNNTs shows an initial decrease at 200 ^{0}C, releasing volatile impurities. After 400 ^{0}C, the mass gradually increased to 130 wt% of the starting sample. This increase indicates the formation of boron oxides, B_2O_3, from the amorphous boron impurities. After 800 ^{0}C, the hexagonal boron nitride (h-BN) and BNNTs are oxidized.
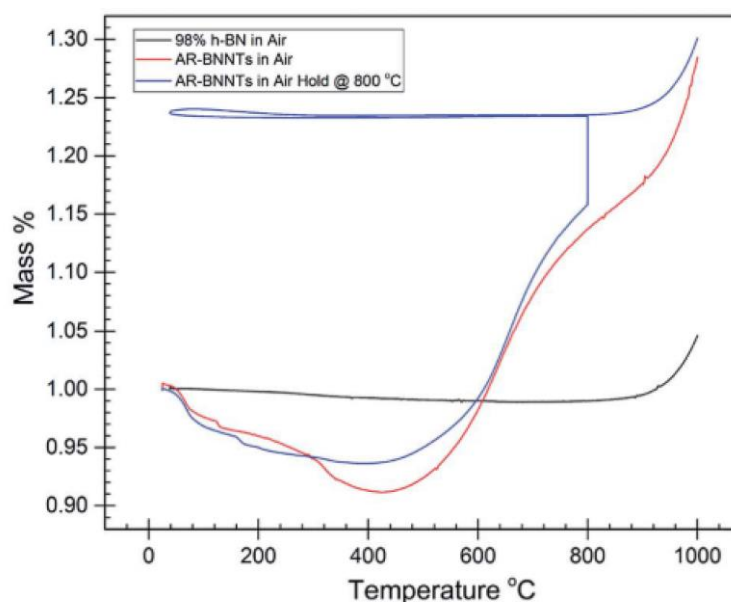
Fig. 1.6 Thermogravimetric analysis of as received BNNTs. Reproduced from Ref. [32] with permissions from Nanoscale Advances and RSC.

The oxides formed after the calcination process are easily removed by washing with warm water followed by filtration. The oxidized and washed (ow-) BNNT samples appear white in color. The remaining impurities are h-BN that are treated more especially due to obtain highly pure BNNT.

1.3.2   Removal of hexagonal boron nitride (h-BN) impurities

Hexagonal boron nitride (h-BN) impurities are harder to remove due to their chemical resemblance to BNNTs. The difference in the density of h-BN and BNNT was taken advantaged to increase the purity of BNNT after the removal of volatile components and boron impurities. Sonication-assisted isovolumetric filtration (SAIF) was used to enrich the BNNT content of oxidized then washed (ow) BNNTs by tip-probed sonication in a mixture of dimethyl formamide (DMF) and acetone[32]. This promotes exfoliation and disaggregation of bundled BNNT and hBN that is separated via vacuum filtration. The difference in the aspect ratio of hBN with BNNT allows the successful removal of h-BN as it is selectively passed through the nanopores of the filter membrane.

The cyclic, π-conjugated surface and defects make it possible to functionalize BNNT. This helps in strategizing separation of h-BN and BNNT improving compatibility of BNNTs in various systems. Different water-soluble surfactants have been previously introduced to the surface of BNNTs to differentiate BNNTs and h-BN.

1.3.3   Functionalization of boron nitride nanotubes

The chemical modification of BNNT is crucial for their successful dispersion into solvents and different matrices like polymers. BNNT surface were successfully modified via covalent and noncovalent functionalization[36–42]. BNNTs were alkylated after reduction with 1-bromohexane as shown in **Fig. 1.7**[38]. Theoretical calculations suggest that reducing BNNTs, i.e. making the

surface negatively charged, would increase their chemical reactivity towards various radicals like •CH$_3$, •NH$_2$, and •OH.
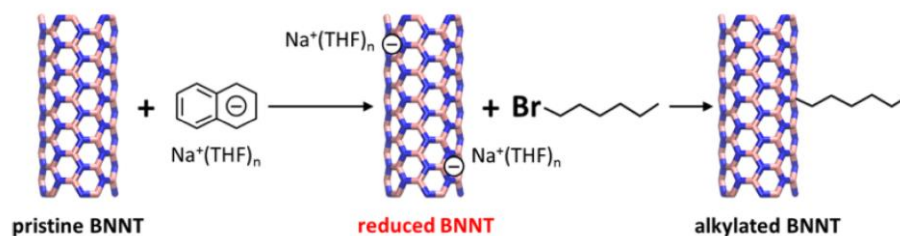
Fig. 1.7 Covalent functionalization of BNNT via reduction chemistry. Reproduced from Ref. [38], from American Chemical Society.

The modification of BNNT via covalent approach increased their reactivity, however such reduction reactions could also alter the inherent properties of BNNT. Early studies have improved the dispersibility of BNNTs in solvents by non-covalent approaches[39,41,43].

Non-covalent functionalization is preferred to keep the high-mechanical strengths and conductivity of CNTs. However, extended to the BNNT system, the approach is limited to a few cases. Using highly conjugated and conductive polymer poly[m-phenylenevinylene-co-(2,5-dioctoxyphenylenevinylene)], (PmPV) in chloroform, BNNTs were successfully functionalized[43]. The π-conjugated rings of BNNT and π-system of the polymer creates an effective π-π stacking interactions between them, forming a homogeneous dispersion of BNNT in chloroform (Fig. 1.8).
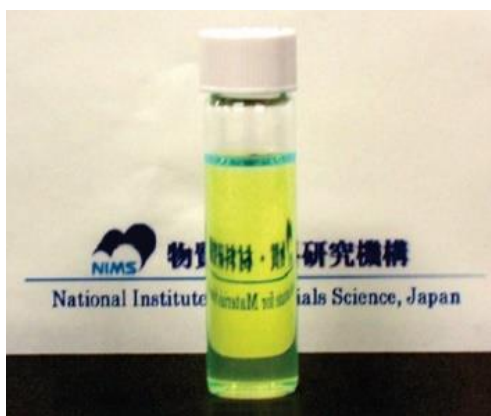
Fig. 1.8 BNNT dispersion using polymer dissolved in chloroform. Reproduced from Ref. [43], from American Chemical Society.

1.3.4   The nanocomposite inks of boron nitride nanotubes

The "dispersion" of BNNT and the "inks" of BNNT will be used interchangeably throughout the manuscript. Inks refer to any mixture containing variety of substances such as solvents, polymers, nanotubes, and other materials. They are used for wide applications such as functional coatings, ink-jet printed films, and paint technologies. The formulation of good inks of BNNTs requires purification and separation of aggregated BNNTs to form a stable suspension of BNNTs in the solution. However, issues arrising from the low purity and poor dispersibility are needed to be addressed first to produced good inks of BNNTs.

The poor dispersibility of BNNTs via direct solvation, or by using a single solvent, leads to the design of various approaches previously discussed. Compared to available CNT processing technologies, the solution processing techniques for BNNT are far way behind. Solid-state applications would require excellent dispersion of the nanotubes, to be

able translate their properties into applications. These fabricated nanomaterials-based products require uniformly distributed composition. Moreover, one-dimensional nanomaterials, in general, are randomly oriented when introduced in nano composites leading to sub-optimal properties. Hence, hierarchical orders like the alignment of nanotubes in fabricated nanomaterials are highly sought for optimum properties.

1.4 Objectives and structure of thesis

Therefore, the objectives of this thesis are:

1. Develop a practical purification route for bulk-produced BNNTs.
2. Design a stable dispersion system for BNNTs.
3. Investigate the assemblies of BNNT in uniform nanofilm deposits.

An introduction to BNNT materials is briefly presented in **Chapter 1**. It includes discussion on the properties, fabrication, purification, and functionalization, stating the primary objectives of the study.

Chapter 2 then proceeds to the development of a purification system producing a stable and uniform dispersion of BNNTs. A solution-based approach is discussed avoiding the energy intensive calcination route. Different dispersion systems, *i.e.* polymer solvent systems are designed using a wide range of solvent.

Chapter 3 then discusses the attempt to improve the alignment of BNNT in uniformly deposited films. In includes high control of the alignment of the BNNT by studying parameters such as polymer addition and substrate treatment. The

chapter also includes a discussion on the alignment quantification technique we employed using high-resolution images run on a software.

Chapter 4 finally gives the summary of the research. Additionally, recommendations and prospects are covered for this emerging nanomaterials.

Chapter 2

Purification and Formulation of the Inks of Boron Nitride Nanotubes (BNNTs)

2.1 Introduction

The application of boron nitride nanotubes （BNNTs） are limited compared to their well-studied carbon nanotubes （CNTs） counterpart, mainly due to the low purity of mass-produced BNNTs and the low selectivity in dispersing BNNTs containing other impurities in almost all solvents[5,36,44].

Recent bulk-production methods produced tubes with significant amount of impurities containing boron and its oxides, and different forms of boron nitride （BN）, most distinguishably hexagonal boron nitride （hBN）, has been proven difficult to remove, due to its chemical resemblance with BNNT[44,45]. Moreover, various researches have focused on the functionalization of the tube's surface with polymers, surfactants, and peptides or biomolecules to enhance its dispersibility in wide range of solvents[36–42]. Here, we report the versatility of a non-aromatic polymer ethyl cellulose （EC） to functionalize and disperse BNNTs.

We will discuss a simplified and more practical approach of the simultaneous purification and dispersion of BNNTs from a bulk-produced source. The results presented in this chapter were published [A] and patented [B] as follows:

[A] De los Reyes FD, Fujieda T, Takeuchi A, Kawai T, Nonoguchi Y. "Isolation of exfoliated boron nitride nanotubes via ethyl cellulose wrapping". Nano Select. 2021; 2(8), 1517-1524 (Wiley, selected as journal issue cover).

[B] 藤枝　正，野々口　斐之，フロレンシオ　デレン　デロス レイエス (Florencio Delen De los Reyes)，河合　壯，竹内　明史，"Method of producing boron nitride nanotubes", Patent No. WO2022/102741, (2022)

2.1.1 Non-covalent functionalization

The functionalization of BNNTs can be done via covalent or non-covalent modifications. Covalent functionalization offers higher reactivity and stability due to the functional moieties chemically introduced to the tube, however, this process alters the intrinsic properties of BNNTs because of significant structural damage during the chemical reactions[38,46]. Hence, non-covalent functionalization is more preferred, employing a simplistic and less destructive approach while maintaining their inherent characteristics[41].

The π-conjugated rings of B=N structure in BNNTs make it possible for small, big, or long molecules to bond non-covalently on its surface via π-interactions. Early studies on the functionalization of BNNTs have used aromatic polymers like poly(m-phenylene-co-2,5-dioctoxy-p-phenylenevinylene) (PmPV) to form dispersion in organic solvents, stabilized by π-π stacking interactions[43]. On the other hand, non-aromatic polymers have been used for non-covalent functionalization of CNTs via CH-π and OH-π interactions. Though effective interactions are expected when highly conjugated polymers are used to functionalize BNNTs, various systems that are widely available and inexpensive are continuously being explored including surfactants and non-aromatic polymers[36].

2.1.2 Ethyl cellulose

Ethyl cellulose (EC) is nontoxic and soluble in various organic solvents. It is also cost-effective and readily available compared to the established highly-conjugated PmPV for dispersing BNNTs[47,48]. It has been previously used by our group, to prepare the inks of CNTs resulting to higher CNT yield and great stability. Furthermore, it is highly flexible with alkyl and hydroxyl groups in its backbone, that makes it a great candidate material to functionalize BNNT surface via non-covalent bonding[49]. In the present study, EC was thus employed and studied in preparing BNNT dispersions in wide range of solvents.

2.2 Materials and Methods

2.2.1 Isolation of BNNTs via EC-assisted dispersion and centrifugation in organic solvents

BNNTs (BNNT-R No. 34235, Tekna Advanced Materials Inc.) were mass-produced based on induction plasma-torch methods with a reported BNNT percentage by weight of approximately 50%, and impurities hexagonal boron nitride (h-BN) and boron oxides of about 30 wt.% and 20 wt.%, respectively. Ethyl cellulose (EC) polymer (45-55 mPa-s, Tokyo Chemical Industry Co.) was dissolved in various solvents such as acetone, benzyl alcohol, butanol, ethanol, methanol, propanol, tetrahydrofuran, and toluene (Wako Pure Chemical Corporation) to prepare the dispersion media, referred here as the polymer-solvent (PolSol) system. In a preliminary experiment, EC samples of different viscosity results in almost the same BNNT dispersions. Therefore, EC (45-55 mPa-s) was conventionally used in the present study.

About 5 mg of the original material was mixed with 20 mL of PolSol system in a vial. The system was dispersed using QSonica ultrasonic dispersion machine and was centrifuged using Kubota 7000 to separate the colloidal dispersion and residue for characterization. The sonication time was varied at 10, 20, 60, and 90 minutes. The centrifugation rate and time were also varied at 10000, 20000 and 30000 relative centrifugal force (RCF); and 60mins, 120mins and 180mins, respectively. The actual photo of the BNNT dispersions was shown in **Figure 2.1**.

The PolSol concentrations were varied from 0.050%, 0.025%, 0.125%, 0.250%, and 0.500% mg EC per mL of solvent used, respectively. For comparison, ow-BNNTs were used in preparing the dispersion using the PolSol system. The percent (%) BNNT in the colloidal dispersion was also analyzed by mass analysis.

Fig. 2. 1 Sample BNNT dispersions at varying EC concentrations, left to right, from 0.500, 0.250, 0.125, 0.060, 0.030, 0.015, and 005 wt.% of EC per solvent (mg/L).

Fig. 2.2 summarizes the flow of the purification process by isolating the polymer-wrapped BNNT from the de-bundled source, dispersed in organic solvents.
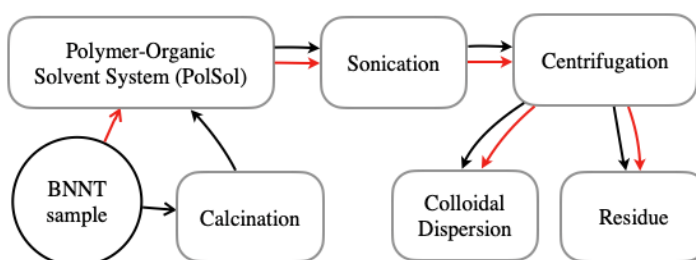
Fig. 2.2 BNNTs were purified directly (red arrow, ➔) without prior heat treatment via mixing followed by centrifugation in the polymer-organic solvent systems. Previously reported purification involves heat-treament before dispersion (black arrow, ➔)

2.2.2 Characterization

Ultra high-resolution field emission scanning electron microscopy (UHR FESEM) was carried out using Hitachi SU9000 equipped with a secondary electron detector. The equipment features superior low-kV performance utilizing in-lens SEM optics and improved vacuum technology. The samples were run using an acceleration voltage ranging from 1 to 5 kV. The samples were prepared by drop casting the BNNT dispersion in a cleaned silicon (Si) wafer which was either dried or calcined prior to imaging.

Transmission electron microscopy (TEM) was carried out using JEOL JEM-3100FEF operating at 300 kV. The samples were prepared by drop casting the BNNT dispersion on a high-resolution copper grid coated with thin layer of carbon for adhesion (HRC-C10 STEM Cu100P).

Fourier transform infrared spectroscopy (FT-IR) measurements were performed using a JASCO 4200 spectrophotometer equipped with a reflection ATR accessory for the powder samples.

The **optical absorption spectra** of the colloidal dispersion were measured using a SHIMADZU UV-3600Plus spectrophotometer.

Thermogravimetric (TG) analysis was conducted on the remaining residue after dispersion and centrifugation, using Shimadzu TGA-60. The temperature was ramped up from 30 $^{\circ}$C to 1100 $^{\circ}$C at 10 $^{\circ}$C min^{-1} with continuous supply of dry air across the sample at 100 mL hr^{-1}. The thermogram profile was used for the percent (%) BNNT dispersion yield calculation via mass analysis.

2.3 Results and Discussion

2.3.1 Morphology of BNNT before and after purification

The mass-produced BNNT source were imaged using scanning electron microscope (SEM) before the purification process. The SEM micrograph of as-received (ar-) materials with reported composition of 50% BNNT, 20% hBN, and 30% other impurities including boron nitride (BN) cages and volatile components, is shown below (**Fig. 2.3a**). After the optimal cleaning process, the purified BNNTs (p-BNNTs) were imaged using SEM and transmission electron microscope (TEM) as shown (**Fig. 2.3b, c, d**). Minimal amount of impurities remained (**Fig. 2.3b**), suggested to be traces of BN cages and nanoparticles, which are attached to BNNTs (**Fig. 2.3c**) making it more difficult to be removed without damaging the nanotubes. BNNT was selectively and individually wrapped by EC (**Fig. 2.4**) which forms a very stable dispersion of BNNT in the PolSol system. The red arrow shows the uniform wrapping of EC, differentiated by TEM characterizations. The wrapping mechanism is provided in **Fig. 2.5**[50].
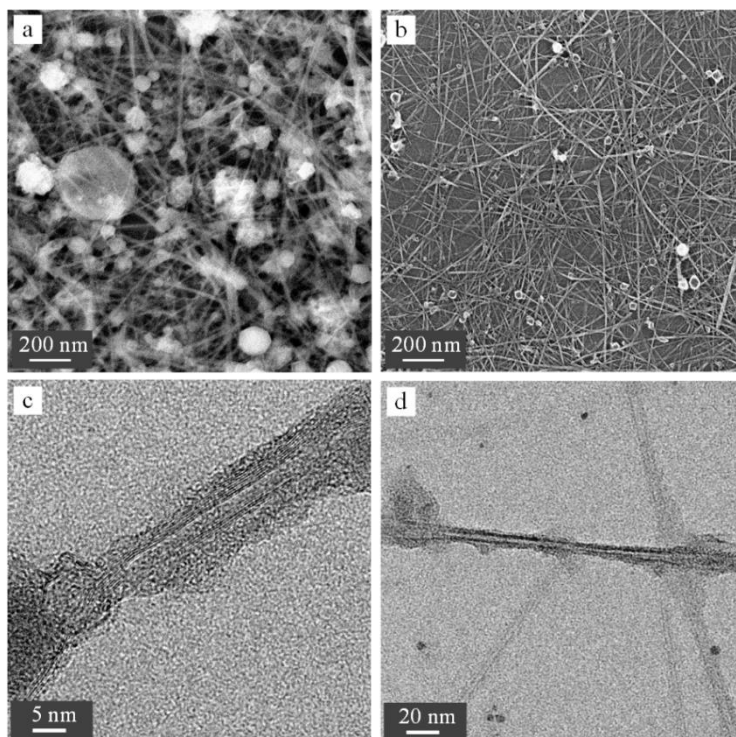
Fig. 2.3 SEM images of (a) as-received BNNTs with impurities, (b) purified BNNTs via dispersion, casted and dried in silicon wafer, and TEM images (c-d) showing individual BNNT wrapped with EC polymer
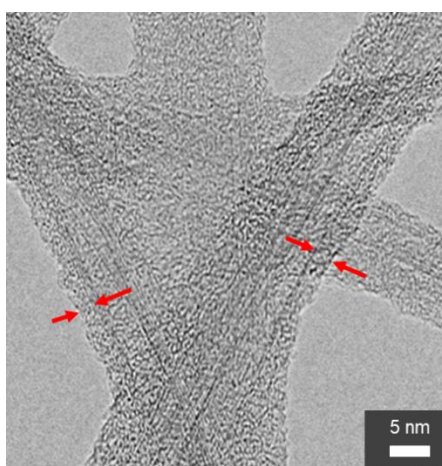
Fig. 2. 4 TEM images of purified BNNTs showing individualized tubes, uniformly wrapped with the dispersant EC indicated by the red arrows.

2.3.2 Functionalization of BNNTs with EC in organic solvents

The ar-BNNT source formed a transparent, yellowish, colloidal dispersion with EC in the polymer-solvent (PolSol) systems after mixing and centrifugation (**Fig. 2.5**). EC is a non-aromatic polymer bearing alkyl and hydroxyl groups in its backbone suggesting that wrapping is due to the CH-π and OH-π interactions between EC and BNNT. These non-covalent bonds can be stabilized by a solvent that can form additional interactions to the tube and polymer. We choose common organic solvents that can all dissolve EC but differs in polarity, hydrophobicity, and aromaticity.
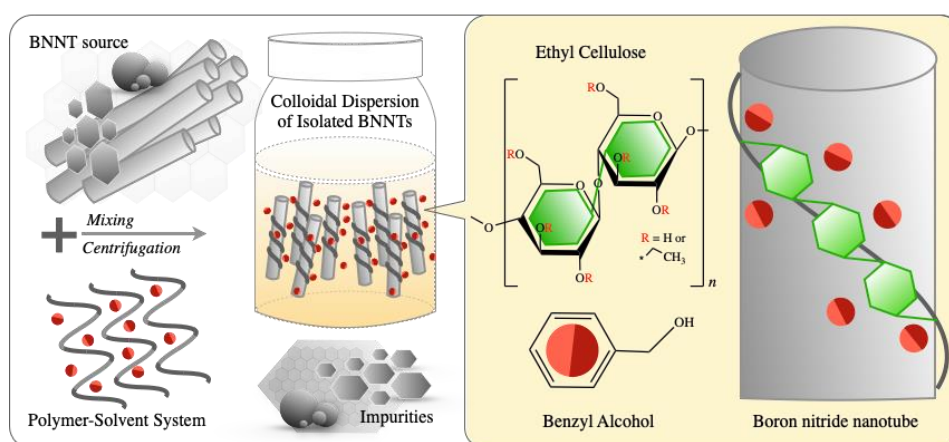
Fig. 2.5 The isolated BNNT after mixing and centrifugation is stabilized by EC wrapped in its surface via non-covalent functionalization, dispersed in BnOH. Reproduced from Ref. [50] with permissions from Wiley and Nano Select.

2.3.3 Absorption of BNNT dispersion using different solvents

The degree of dispersibility of BNNT was highest in the EC-benzyl alcohol (BnOH) system based on the UV-Vis absorption spectra of the dispersion obtained from 300-600 nm (**Fig. 2.6A**), where absorbance is expected

32

proportional to solute concentration on the basis of the Lambert-Beer's law. BnOH possesses polarity and aromaticity, capable of forming H-bonding and hydrophobic interactions with EC. BnOH can also adsorb in the unwrapped or exposed surface of BNNT held by π-π interactions when the aromatic ring is oriented towards the tube. In addition, the polarizability of the B-N bonds in BNNT can offer additional N-H interactions, adding stability to the dispersion system.
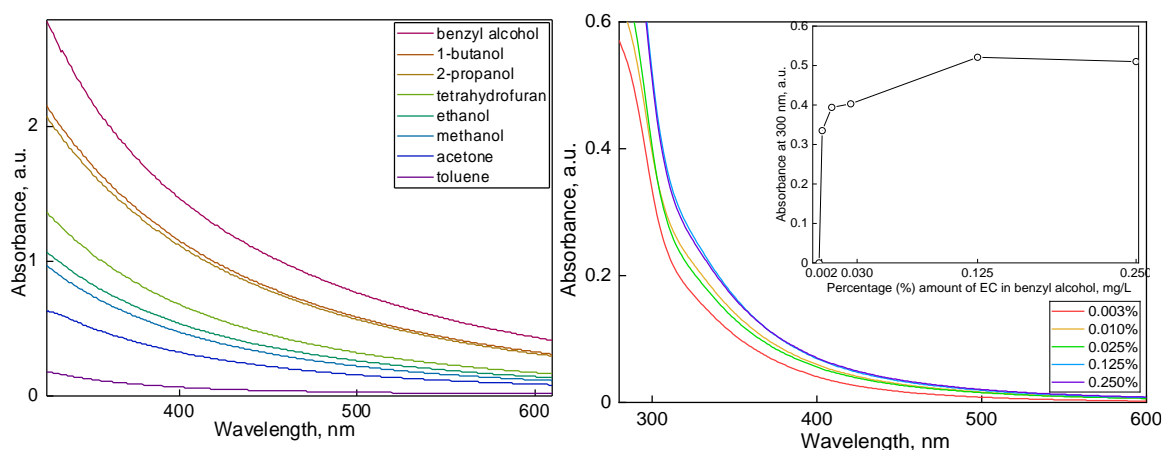
Fig. 2.6 UV-Vis absorption spectra of (A) BNNTs dispersed in EC dissolved using common organic solvents and (B) BNNT dispersion at increasing concentration of EC using BnOH as solvent, with inset absorbance values versus different EC concentrations, of the dispersion at 300 nm.

The optimum amount of EC needed to disperse the maximum amount of BNNT in a fixed volume of BnOH was also determined from the UV-Vis absorption spectra of BNNT dispersions at varying PolSol concentrations, measured from 300-600 nm (**Fig. 2.6B**), with inset absorbance values versus different EC concentrations, of the dispersion at 300 nm. At 0.125% mg EC per mL of a solvent used, the maximum absorbance was observed indicating the maximum amount of the EC-wrapped BNNT in the PolSol system.
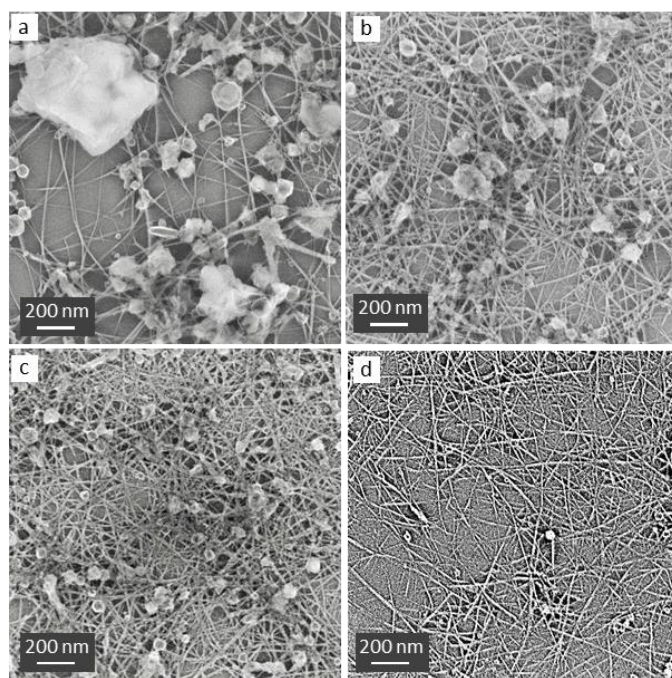
Fig. 2.7 SEM images of BNNTs (a) before purification, and after centrifugation at (b) 10,000, (c) 20,000, and (d) 30,000 applied relative centrifugal force to the BNNTs wrapped with EC in benzyl alcohol.

2.3.4 Effect of sonication and centrifugation on BNNT dispersion

The applied centrifugation rate on the BNNT dispersion after mixing was varied using the optimum concentration of PolSol system. Before centrifugation, the ar-BNNT source contains bundles and aggregates of BNNT, hBN, and B oxides as shown in the SEM image (**Fig. 2.7A**). The certificate of analysis reported about 50% BNNT, 30% h-BN and 20% B and oxides, contained in the ar-BNNT source. Upon increasing centrifugation rate from 10,000 to 30,000 relative centrifugal force (RCF), the amount of impurities is reduced significantly (**Fig. 2.7B, C, D**). Very minimal impurities of less than 40 nm diameter are noticeable after applying 30,000 RCF where the size distribution of the traces of impurities becomes narrow (**Fig. 2.8**).

These impurities were further reduced when the centrifugation time was increased from 60 to 180 minutes (**Fig. 2.9**). The effect of varying sonication time examined at 10, 20, 60, and 90 minutes (**Fig. 2.10**) showed that de-bundling with minimal destruction was achieved using the shortest time, therefore all the dispersions were sonicated for 10 minutes to avoid possible damage on the tubes during mixing. It is noteworthy that the BNNT used in preparing the dispersion systems were provided by two companies, BNNT-R Tekna and BNNT LC.
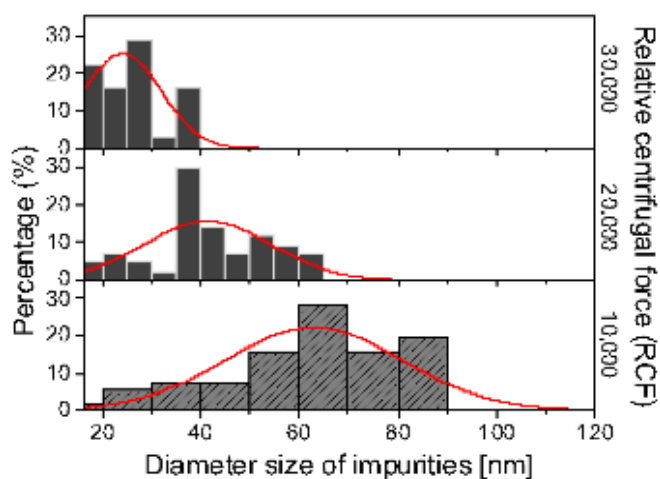
Fig. 2.8 Size distribution of the remaining impurities at increasing relative centrifugal force (RCF) applied to the BNNT dispersion
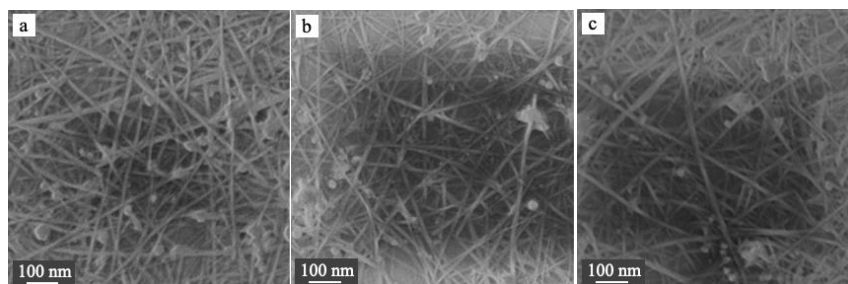
Fig. 2.9 SEM images of the colloidal dispersion after (a) 60, (b) 120, to (c) 180 minutes centrifugation time at 30,000 applied RCF

2.3.5 Quantification of purity via FTIR methods

The FT-IR spectra of the as-received (ar-) and purified (p-) BNNT are shown below (**Fig. 2.11A,F**). After the purification, p-BNNT shows distinct peaks centered at 1366 and 811 cm^{-1}, corresponding to the in-plane B-N optical mode (TO) and the B-N-B out-of-plane buckling modes (R) of BNNT, respectively[37,51]. This shows almost similar peak positions to ar-BNNT but with evident differences on the general shapes, height, and width of the peaks. A broader peak from 1600 to 1200 cm^{-1} is observed for the ar-BNNTs, explained due to the overlap of the tangential and longitudinal frequency modes of B-N bonds from BNNT and the impurities present, mainly hBN[52]. The narrowing and increase in the symmetry of the peak of p-BNNT suggests an increase in the purity of BNNT after the isolating the EC-wrapped BNNT from the source. The observed shift in the absorption of ar-BNNT from 803 to 811 cm^{-1} of p-BNNT also supports this increase in purity of BNNT, similar to the recent studies of Harrison *et. al* on FT-IR spectroscopy technique for the quantification of hBN impurities in BNNTs[32]. They showed that the height ratio of the peaks at 780 and 1327 cm^{-1}, corresponding to the R and TO modes, respectively, shows direct proportionality to the amount of hBN.
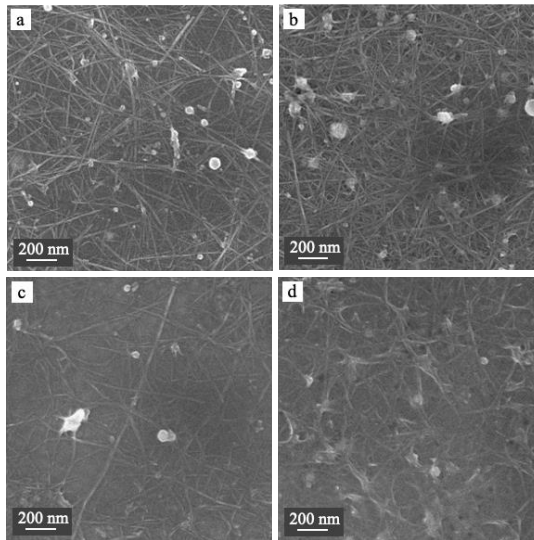
Fig. 2.10 SEM images of the colloidal dispersion after (a) 10, (b) 20, (c) 60, and (d) 90 minutes sonication time.
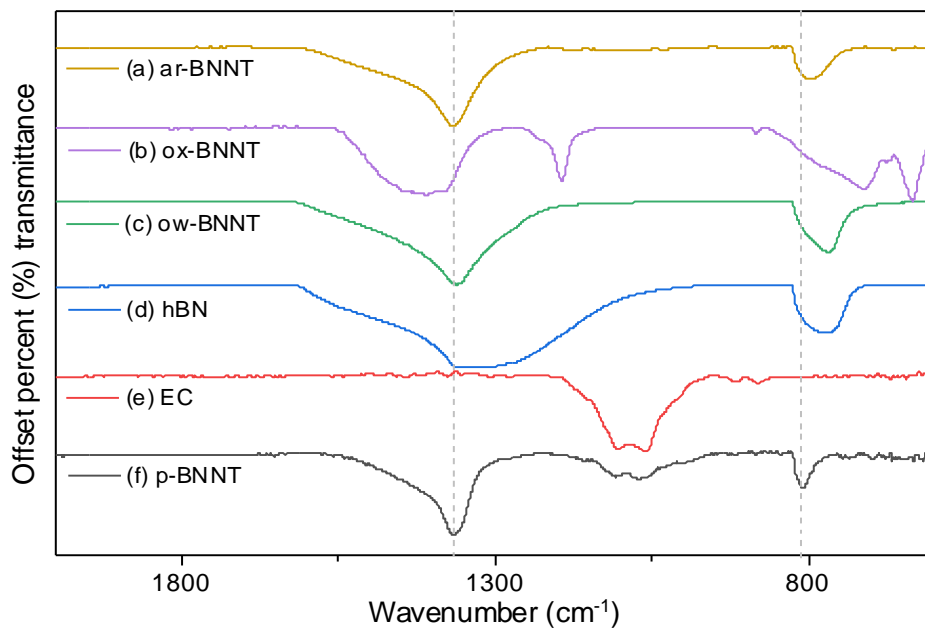
Fig. 2.11 FT-IR spectra of hexagonal boron nitride (hBN) and as-received (ar-), oxidized (o-), oxidized-washed (ow-) and purified BNNTs.

BNNTs were isolated (p-BNNT) from unpurified source (ar-BNNT) without any other pre-heat treatment as reported earlier where boron impurities are converted first to its water-soluble oxide form (ox-BNNT) for easier removal by water or ethanol washing, leaving only the mixture of hBN and BNNT (ow-BNNT)[35]. Therefore, we only considered the R/TO ratios of the ow-BNNT and p-BNNT reliable (**Table 2.1**), as there are no overlapping FT-IR absorptions in their R and TO peaks, aside from the absorptions from BNNT and hBN. A decrease in the R/TO ratio of the isolated BNNT, down to 0.32, implies a significant removal of hBN, hence enhancement in the purity of BNNT which is also confirmed from our high-resolution electron microscope images.

Table 2.1. B-N-B out-of-plane and B-N in-plane mode ratio, R/TO, of samples containing BNNT.

Samples	R/TO ratio
ar-BNNT	0.35
ox-BNNT	0.42
ow-BNNT	0.49
p-BNNT	0.32

2.3.6 BNNT yield calculation via TGA methods
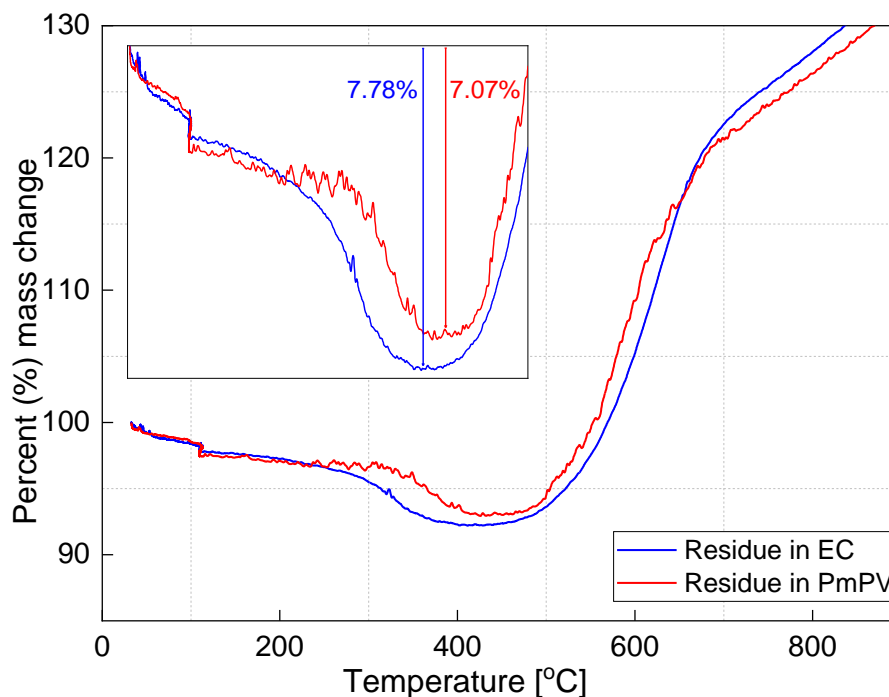
Fig. 2.12 TG analysis curve of recovered residue of BNNT mixtures in (a) ethyl cellulose (EC), and (b) poly(m-phenylene-co-2,5-dioctoxy-p-phenylenevinylene) (PmPV)

Finally, the amount of the BNNT dispersed in the PolSol system was quantified using mass conversion measurements based on the paper by Smith McWilliams *et al.*[36]. The residue after the centrifugation process was carefully separated from the colloidal dispersion, dried, weighed, and characterized using thermogravimetric (TG) analysis to calculate the amount of BNNT retained in the PolSol system (**Fig. 2.12**). Using EC-BnOH, approximately 55% by mass of BNNT was retained in the colloidal dispersion using our optimum conditions (10 minutes sonication time and

30,000 RCF for 180 minutes). This is higher compared to the dispersion we prepared using a highly conjugated polymer, poly(m-phenylene-co-2,5-dioctoxy-p-phenylenevinylene) (PmPV)[43], with a 42% dispersion yield, using chloroform ($CHCl_3$) as a solvent. This is supported, qualitatively with the SEM images (**Fig. 2.13**) of the colloidal dispersion showing more BNNT in the EC-BnOH than the PmPV-$CHCl_3$ system. The SEM sample was prepared using 30 µL of the colloidal dispersions, casted and dried in a 20x20 mm^2 cleaned Si wafer for a more reliable comparison.
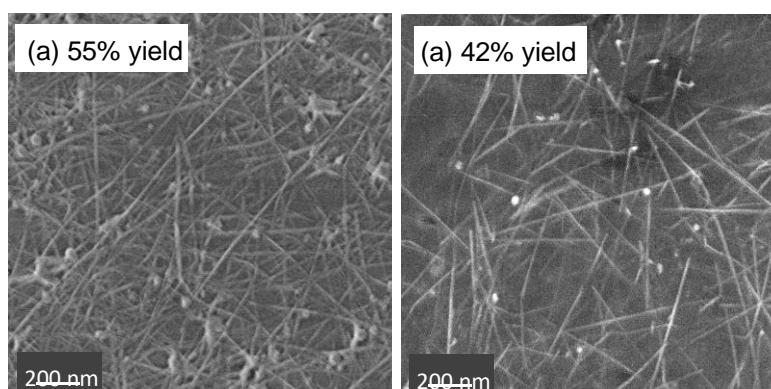
Fig. 2. 13 SEM images of colloidal dispersion prepared using (a) a non-aromatic EC and (b) a highly-conjugated PmPV

2.5 Conclusion

The enhancement in the purity of BNNT, simultaneously de-bundled and dispersed in a non-aromatic polymer-organic solvent system was successfully achieved and reported from this work. The stable colloidal dispersion contained highly pure individualized BNNT with very minimal trace of nanosized hBN impurities, qualitatively and quantitatively supported by comprehensive characterizations including FESEM and TEM images, UV-Vis and FT-IR spectra, and TG analyses. Our method using the polymer EC has provided us a deeper insight to the versatility of using nontoxic, widely available, and inexpensive non-aromatic polymeric systems, further amplified by a chosen solvent, to enhance the dispersibility and stability of sorted BNNTs in the system. In particular, using a simplified and less destructive approach without heat treatment, we have isolated and dispersed individual nanotubes in our designed system. This contribution in the solution-based processing of BNNTs, using EC dispersant in various solvents, can provide a wider range of applications specifically for production of composite materials that requires large amount of high-quality BNNTs.

Chapter 3

Alignment Studies of Boron Nitride Nanotubes (BNNTs)

3.1 Introduction: Evaporative-driven hierarchical assemblies of BNNTs

Boron nitride nanotubes (BNNTs) are ideal reinforcing fibers for composites for extreme applications because of their exceptional mechanical properties, and superior thermal conductivity, on top of their inherent piezoelectric properties and neutron absorption capability. For example, using BNNT as reinforcements in composites has increased their mechanical strength and thermal conductivity[53–56]. The behavior of the composites depends on the spatial control and dispersion of the individual nanotubes, like BNNTs or CNTs, in the matrix, such as polymer[57–59].

The hierarchical organization, i.e., alignment or unidirectional orientation of nanotube systems like BNNTs and CNTs, in composites has improved their performance[60–66]. This chapter will discuss the successful fabrication of BNNT-based films showing uniform deposits of highly aligned BNNTs, via evaporative-driven mechanisms. The well-studied carbon nanotube system will be the major basis of the alignment studies of BNNTs. Moreover, the uniform film deposition will be modulated based on the coffee-ring effect (CRE) phenomenon.

Controlling the coffee-ring effect towards uniformly deposited films

The evaporation of sessile drops containing dissolved or suspended particles leaves ringlike structures on surfaces. A ring-like stain is observed when a drop of coffee is left dried on paper. This refers to the natural phenomenon known as the coffee ring effect (CRE). The ring-like deposit is formed if the contact line of the

evaporating drop is fixed or pinned[67–69]. The outward capillary flow driven by the surface tension as solvent is evaporated, carries the suspended particles to the periphery of the sessile drops. CRE includes not only coffee but any fluid involving a drying sessile drop containing non-volatile compounds like blood, inks, paints, and solutions of polymers, nanoparticles, or nanofibers[69,70]. Many industrial processes depend on uniform deposits of non-volatile components, hence efforts have focused on the modulation of the CRE to obtain homogenous patterns, rather than peripheral rings[67,71–75]. A sugar-assisted uniform patterns of coffee powder was obtained at a threshold sugar concentration[71]. The CRE pattern can be suppressed via occurrence of depinning contact line, disturbing the outward flow via Marangoni, or prevention of particles to transport to the edge. During evaporation, the transport of suspended compounds depend on the size[76,77]. Smallest particles were observed on the outermost periphery of the deposits followed by bigger particles. An order to disorder arrangement of this particles with different size was observed via scanning electron microscopy. Generally, controlling deposits requires multi-step procedures or expensive equipment to achieve uniform patterns[73,78,79]. Hence, this chapter attempts to form uniformly distributed and well-aligned BNNT in deposited films with conventional solvent evaporation process.

The alignment of the nanotubes will be analyzed and quantified via image analysis, using software applied previously to networks of one-dimensional systems such as collagen fibers and poly vinylidene fluoride-based polymer composites[80–82]. To the best of my knowledge, the image-based analysis procedure[83] has not been reported and applied to nanotube system.

3.2 Materials and Methods

3.2.1 Preparation of BNNT dispersion

The dispersion of BNNT was prepared using polymer as dispersant in an organic solvent system. 5 mg of BNNT (BNNT-R No. 34235, Tekna Advanced Materials Inc.) was added in a solution containing polyvinyl butyral (PVB). Similar to the EC system, PVB was chosen due to its cost-efficiency, availability and wider solubility in many organic solvents. Common organic solvents such as acetone, benzyl alcohol, ethanol, methanol, tetrahydrofuran, and toluene (Wako Pure Chem. Corp.) were used to prepare the polymer solution. The solution was sonicated using QSonica tip-probed dispersion machine for 20 minutes; after which a stable BNNT dispersion was collected by centrifugation at 30,000 relative centrifugal force (RCF) for 3 hours. The BNNT dispersions were prepared at 0.005, 0.025, 0.125, 0.250, and 0.500 wt% of PVB per 20.0 mL of the solvent. The BNNT films were fabricated using these dispersions.

3.2.2 Fabrication of BNNT film

The films of BNNT were fabricated by drop casting method. The dispersion of BNNT was dropped in a 10x10 mm^2 cleaned silicon substrate. The solvent was evaporated at a temperature above its boiling point. Slower heating rate (5 ^{o}C/min) kept up to the drying temperature and was kept for 3 hours prior to characterization. Multilayer deposited BNNT films were also fabricated by repeated drop casting of the BNNT dispersion.

3.2.3 Morphology Characterization

The structure and morphology of the film was investigated using Hitachi SU9000, an ultra-high-resolution field emission scanning electron microscope (UHR FESEM) equipped with a secondary electron detector. The nonconductive films of BNNT-polymer hybrid were imaged using an acceleration voltage between 1 to 5 kV, without prior coating. The equipment can obtain high-resolution images at lower kV requirement by utilizing in-lens optics and improved vacuum technology. Multiple SEM images with varying field of view (FOV) were acquired at different areas of the film including the center, near the center, and edges of the film for alignment investigation.

3.2.4 Alignment Quantification

The alignment of BNNTs in drop-cast films was quantified using image analysis. The Image-Based Fiber Orientation Calculator (Academic Use License) using MATLAB, developed by University of Minnesota (reference) was used in the analyses. The acquired FESEM images were pre-processed by cropping into a square dimension and removing areas with scale bar, text, and noise, for a more accurate results. The degree of alignment is calculated from the orientation matrix generated from the MATLAB algorithm, discussed in the previous chapter.

3.2.5 Mechanical Scratching via Soft-friction Transfer Method

The aligned gratings on the cleaned silicon substrate was introduced by brushing the surface with a cellulose membrane based on previously reported method[84]. The mechanical scratches contains cellulose that can serve as template for molecular alignment. For comparison, a brushed substrate was cleaned again before deposition. The aligned BNNTs on non-brushed, brushed, brushed then washed substrate was investigated.
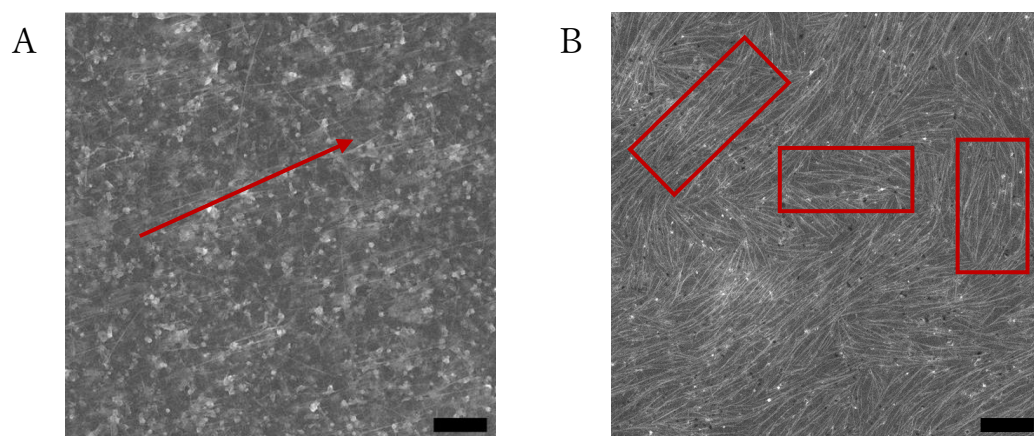
Fig. 3. 1 Preliminary observation of alignment of BNNT in drop cast film with polyvinyl butyral (PVB): dispersions centrifuged at (A) 20,000 vs (B) 30, 000 x g rate. [Scale: 2 μ m]

3.3 Results and Discussion

Fig. 3.1A shows the SEM image of a drop cast and dried dispersion of BNNT in PVB dissolved in benzyl alcohol, BNOH, along with other impurities. The image shows high order assemblies of BNNT and PVB after solvent evaporation which was clearly revealed in **Fig. 3.1B** upon the removal of the impurities. The group or arrays of BNNTs oriented in one direction, enclosed in box, were observed for the first time when we introduced PVB in our dispersion sytem.
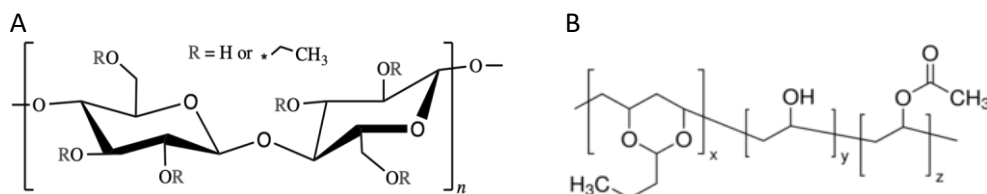
Fig. 3. 2 Structure of ethyl cellulose (A) and polyvinyl butyral (B)

PVB contains butyral, alcohol and acetate side groups compared to the alkyl and hydroxyl group of EC (**Fig. 3.2**). The relative amounts of the side groups can be controlled in PVB but they are generally distributed throughout the chain. They are used primarily for applications that require strong binding due to their high flexibility and stronger interactions[85]. The aliphatic backbone supporting Van der waals interactions and the oxygen-bearing sidegroups capable of stronger polar interactions, suggest the formation of the strong BNNT/PVB assemblies. The high order assemblies of BNNT/PVB was not observed in BNNT/EC.

The heterogeneous deposited BNNT film resulting from the evaporative-driven coffee ring phenomenon shown in **Fig. 3.3A** surprisingly produced arrays of aligned BNNT-PVB assemblies. Hence, the CRE patterns and corresponding nanomorphologies at different concentrations of PVB were investigated.

3.3.1 BNNT/PVB Coffee-ring pattern: Effect of concentration

Fig. 3.3 shows patterns of the BNNT/PVB assemblies at increasing concentrations of PVB. The BNNT dispersion contains 0.005, 0.025, 0.125, 0.250, and 0.500 wt.% of PVB in benzyl alcohol. After drop casting a 10 μL of the dispersion, circular patterns of about 7 mm in diameter was observed. Our previous results show that for 20 mL volume of the dispersion the optimum amount of dispersed BNNT is reached at 0.125 wt.% of the dispersant. The pattern with the lowest PVB concentration shows a peripheral ring with uneven and heterogeneous deposits concentrated on the left portion of the circle. Increasing the concentration by five times (5x) has completely covered the circular pattern.

Fig. 3. 3 Coffee ring patterns of drop cast BNNT prepared with increasing concentrations of PVB/BnOH system:

(A) 0.005% (B) 0.025% (C) 0.125% (D) 0.250% and (E) 0.500%
[**Scale**: 1 mm]
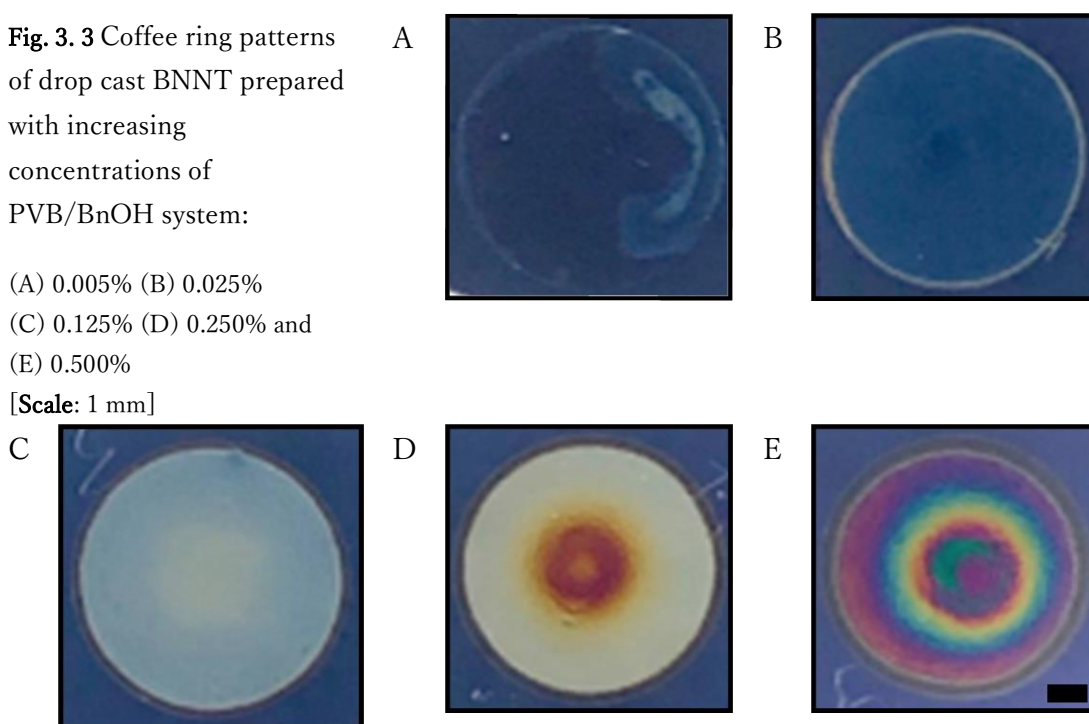
At 0.125 wt.%, uniformly deposited film was obtained in which, deposits appear to start concentrating in the center of the pattern. At 0.250 wt.%, the BNNTs starts to build up, shown as the yellowish deposits. Interestingly, concentric circular rings indicated by different colors in the pattern was obtained at the highest amount of the surfactant used.

Image intensity profile: Uniform film deposits analysis

The analysis of the intensity of the deposited materials was done by linearly profiling the pixels of the acquired images. All the images were converted to grayscale prior to intensity analysis using ImageJ software. The plots of the grayscale value versus distance in pixels unit were shown in **Fig. 3.4**. The fluctuations in the grayscale values of the intensity profile plots indicate non-uniform deposition of the BNNT over the substrate. For example, **Fig. 3.4A** shows the appearance of two peaks between 100-150 pixel distance. These peaks indicate the heterogeneous and uneven deposits of the materials at those areas. **Fig. 3.4B**, on the other hand, shows two peaks at distance near 0 and near 150, corresponding to the peripherical or outer ring of the deposits. Between 0 and 150 pixels, there is a uniformly, thin deposits of BNNTs in the substrate.

The uniformly deposited BNNT films at 0.125 wt.% of PVB was confirmed best using the intensity profile characterization (**Fig. 3.4C**). Compared to other plots, it shows a "thick" deposits between the peripheral rings, shown by a higher grayscale values between 0 to 150 pixel distance.
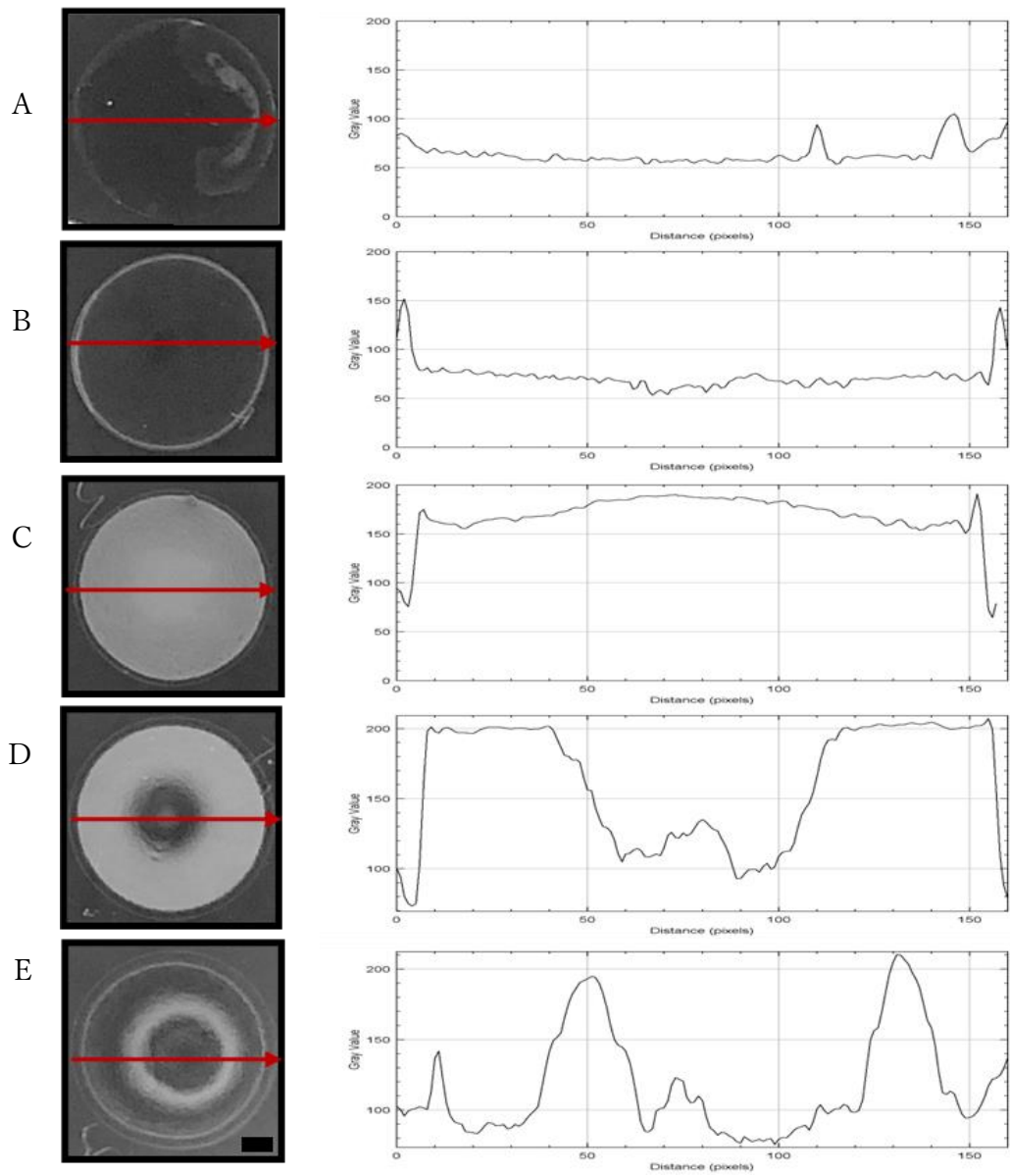
Fig. 3. 4 Intensity profile characterization of BNNT films containing increasing PVB concentration
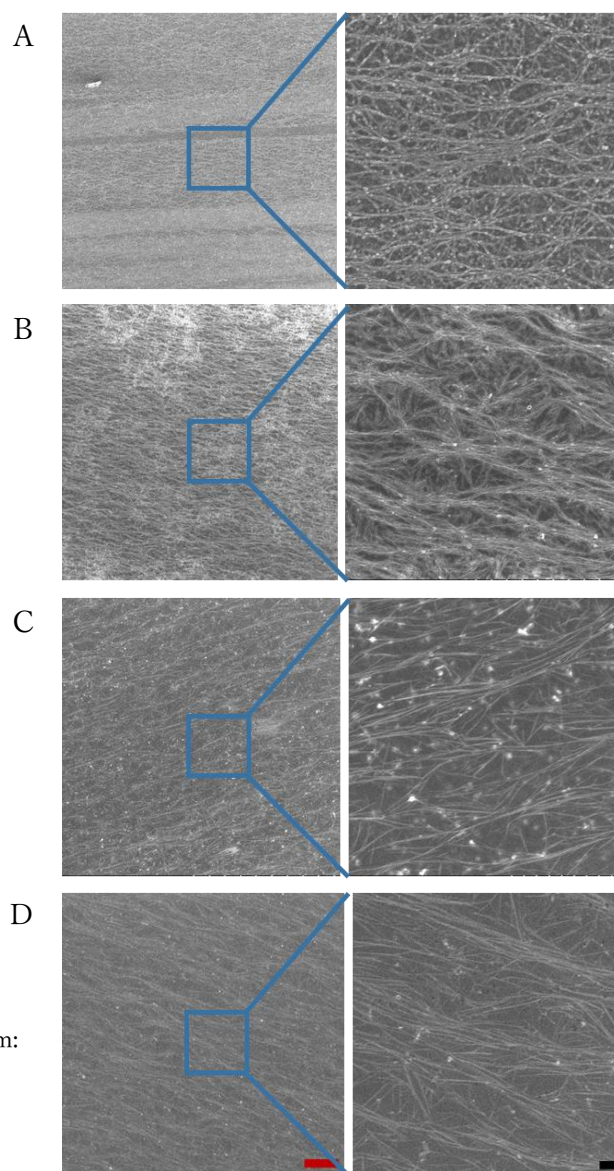
Fig. 3. 5 SEM images of BNNT prepared with increasing concentrations of PVB/BnOH system: (A) 0.005% (B) 0.025% (C) 0.125% (D) 0.250%

[**Scale:** 2 μ m; 400 nm]

The morphology of the nano-assemblies is shown in **Fig. 3.5**. The area between the center and the periphery of the ring was imaged using SEM, at low and high magnifications. All the nano-assemblies shows ordered BNNT in the deposited films. However, a more regular pattern is obtained at concentrations higher than 0.025 wt.% PVB.

3.3.2 Investigating alignment of BNNT in the coffee ring

Further analysis of various areas in the pattern reveals interesting organization of the BNNT system in the assemblies. **Fig. 3.6** shows different areas, used in SEM imaging, labeled A to G. The film was fixed in the aluminum holder of the SEM equipment, scanned, and imaged for comparison. The SEM images are shown in **Fig. 3.7**.
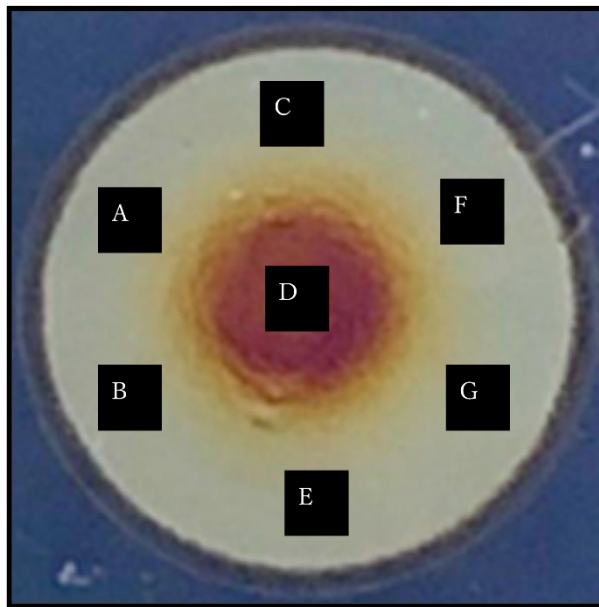
Fig. 3. 6 Marked areas on the BNNT films analyzed using high-resolution scanning electron microscopy
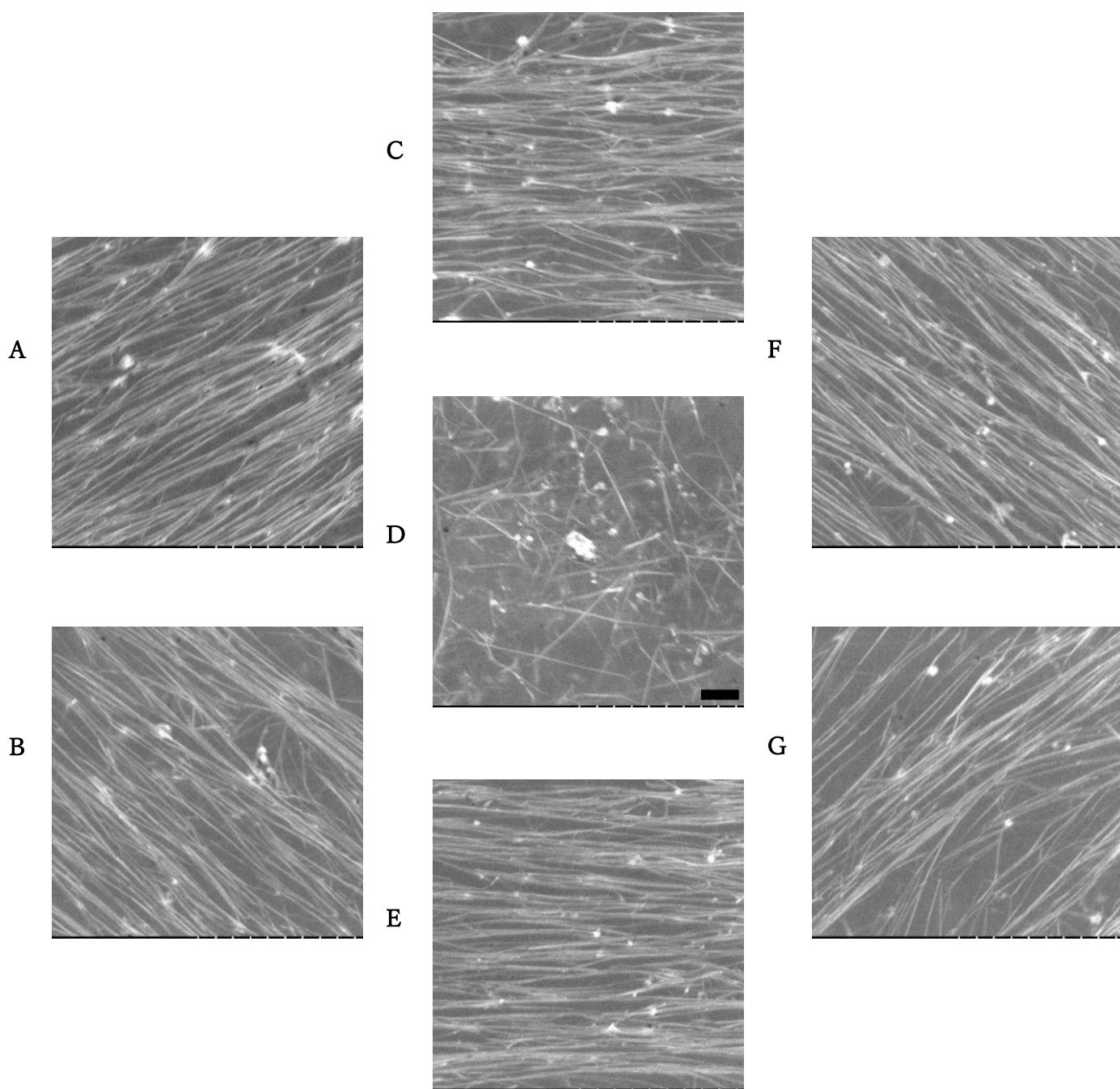
Fig. 3. 7 Scanning electron microscopy (SEM) images of BNNT at various areas of the coffee-ring effect. The label (A-G) corresponds to the area marked in **Fig. 3.6**.

[**Scale:** 200 nm]

The areas imaged at higher magnification contains an ordered arrangement of BNNTs that follows a concentric manner. Horizontally aligned BNNTs are shown in **Fig. 3.7C,E**. On the other hand, **Fig. 3.7A, B, F, G** shows oriented BNNT at $\pm 45^0$C orientation relative to the horizontally aligned BNNTs. The center of the pattern, **Fig. 3.7D** shows random arrangement of BNNTs. Previous studies on the coffee ring patterns obtained using binary mixtures of nanoparticles reveals high ordered arrangements of the nanoparticles (NPs) near the periphery, with larger diameter NPs located near the center of the pattern[77].

As the non-volatile components flow outward because of the higher rate of evaporation near the edge of the drop-cast dispersion, the impurities remaining in the dispersion containing boron NPs and nano-sized hBN travel faster towards the periphery forming the circular outline visible in the patterns, **Fig. 3.6**. The presence of PVB also avoids pinning of the contact line resulting to uniformly distributed BNNTs in the pattern. Previous approaches suppressed the heterogenous deposits by using surfactants for depinning the contact line[71,74,75]. The surfactant used in our dispersion system, PVB, allows both uniform deposition of the suspension in the substrate and alignment of BNNTs between the center and the edge of the patterns. The areas where high ordered alignment observed is quantified using image analysis software that gives the degree of

alignment, the magnitude and direction, and the distribution orientation of the BNNTs.

3.3.3 Alignment Evaluation: Techniques

The evaluation of morphologies of nanostructures including CNTs and BNNTs is commonly done using microscopy techniques. Atomic force microscopy (AFM), scanning tunneling microscopy (STM), transmission electron microscopy (TEM) and scanning electron microscopy (SEM) are used in the analysis of nanotubes alignment[86–88]. The limitation on the sampling area and the complicated sample preparation with TEM make it less suitable for such analysis, compared to AFM and SEM. Spectroscopic methods are also well-established techniques relying on the preferential absorption, scattering, or emission of light polarized along the axes of 1D nanostructures[57,89–92], such as Raman scattering which has been useful in determining the degree of alignment (S_{2D}) of anisotropic sw-CNT[89].

The dependence of the G band, at 1590 cm^{-1}, on the molecular orientation of CNT is useful on their orientation analysis. The change in the Raman peak is due to the presence of the longitudinal face of the aligned CNTs. Similarly, Raman studies for sw-BNNT showed the most intense peak at 1365 cm^{-1} [93,94]. This peak also corresponds to the Raman optical E_{2g} mode of the impurities h-BN commonly encountered in BNNT samples. The observed Raman peak ratio for BNNT of 2.4:1[91], due to alignment is relatively lower than the Raman peak ratio of CNT fiber of 5.1:1[92]. Moreover, contradicting results were previously reported on the Raman peaks of BNNTs due to the diversity in structures including diameter and

number of walls, as well as traces of h-BN[93]. Thus, Raman signals of BNNT are not reliable enough to characterize their alignment or molecular orientation. Therefore, our investigation of the alignment of BNNT films focuses mainly on studying high-resolution SEM images.

3.3.4 Image-based Alignment Quantification

Image-based measurements for determining various structural features such as diameter, length, thickness, and orientation have been useful in various structure-property relationship analyses specially in the nanoscale level[81–83]. Fiber network orientation of collagen and other tissue analogs have been analyzed using different image-based measurements such as mean intercept length (MIL), line fraction deviation (LFD), and Fourier transform method (FTM). The accuracy of these methods to analyze parameters is important for the improved performance of the system under study.

The accuracy and efficiency of MIL, LFD and FTM orientation measurements methods have been studied using various randomly generated images containing 1D networks in Matlab[83]. FTM method outperformed MIL and LFD in terms of both accuracy and calculation time. Therefore, we extend the FTM method in the alignment studies of BNNT-based films.

3.3.5 Fourier Transform Method (FTM)

The accuracy and efficiency of MIL, LFD and FTM orientation measurements methods have been studied using generated images containing 1D networks that differs in the alignment (**Fig. 3.8**). The corresponding

calculated distributions using the three methods were compared to the network distribution of the generated image. In all three cases; (A) highly aligned network, (B) network with some alignment, and (C) a nearly random network, the FTM resulted the best agreement to the test images.
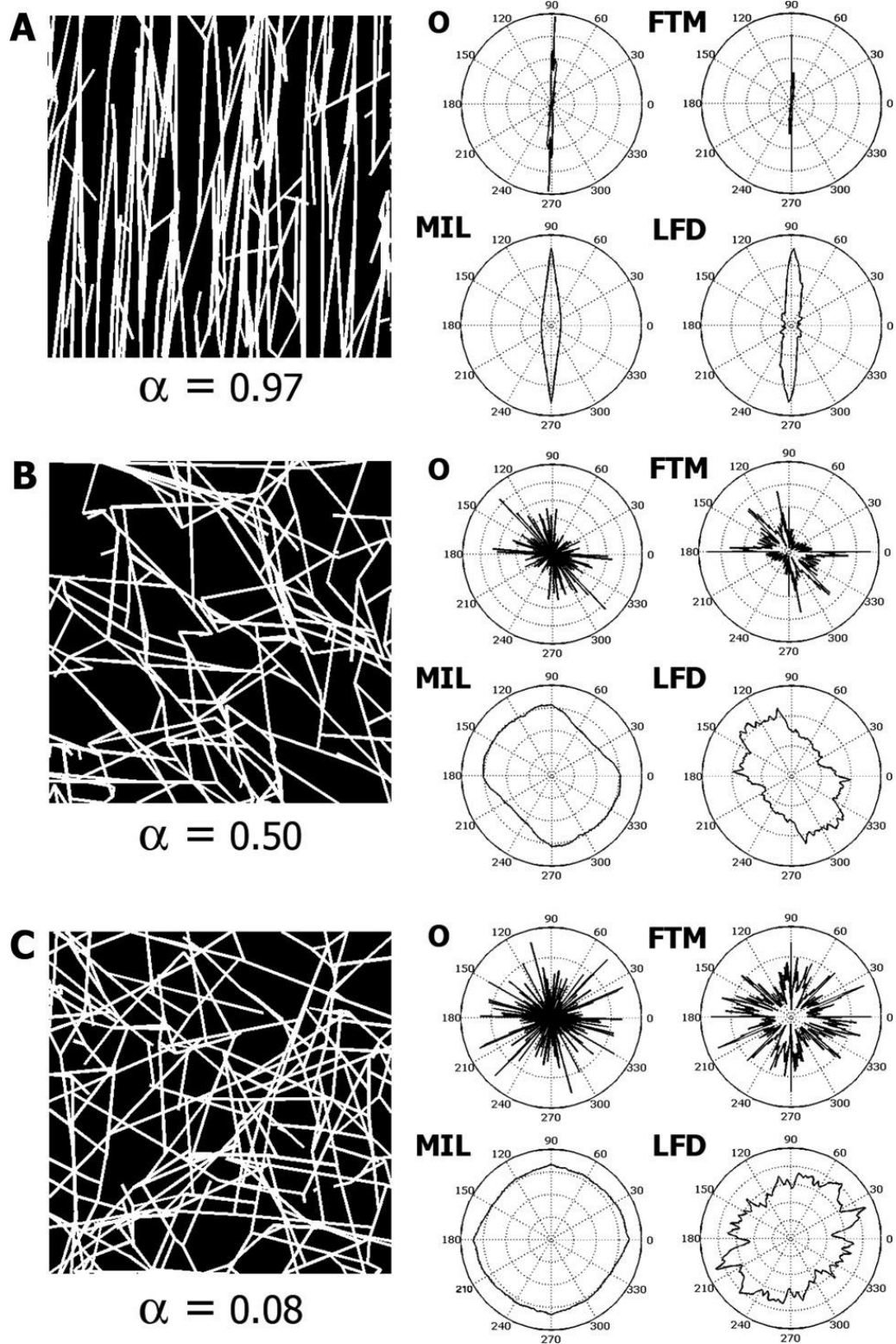
Fig. 3. 8 Comparison of the MIL, LFD, and FTM methods. Reproduced from Ref. [83], with permission from Wiley and Journal of Bio. Mat.

3.3.6 Grayscale Image Processing

Fourier transform method (FTM) can reduce complex spatial information contained in a digital image in terms of computer processable data. A digital image is composed of pixels that differ in intensity. **Fig. 3.9** is an example of a binary image in which pixels has one of only two discrete values: 1 or 0. This type of image processing is usually used to identify the region of interest in the image.
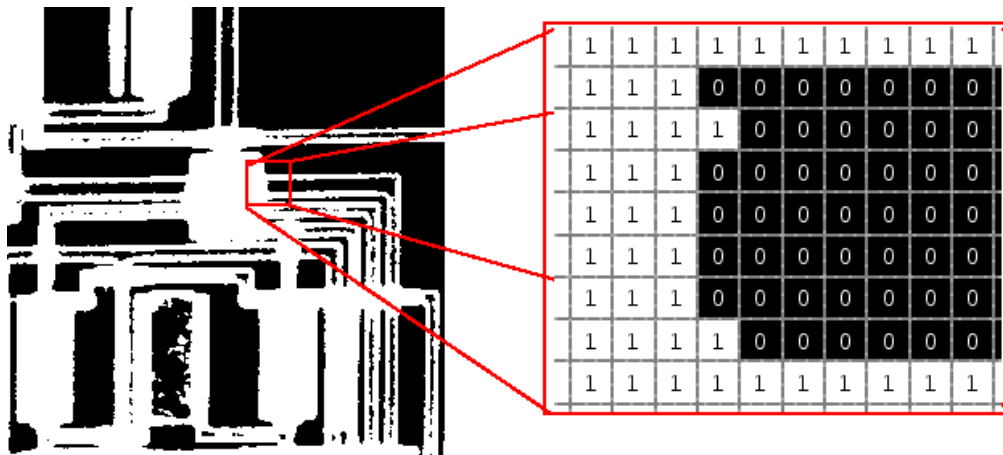
Fig. 3. 9 Binary image processing. Image reproduced from Mathworks Image Processing Toolbox, accessed 2022.

On the other hand, a grayscale image (**Fig. 3.10**) contains data representing the intensity per image pixel, values range from 0 to 1. Matlab software allows user to customize the color map to represent the color intensities contained in the image. In a grayscale SEM image containing nanotubes, the rapid change in the intensity indicates object edges that can be used for quantitative analysis of their orientation.
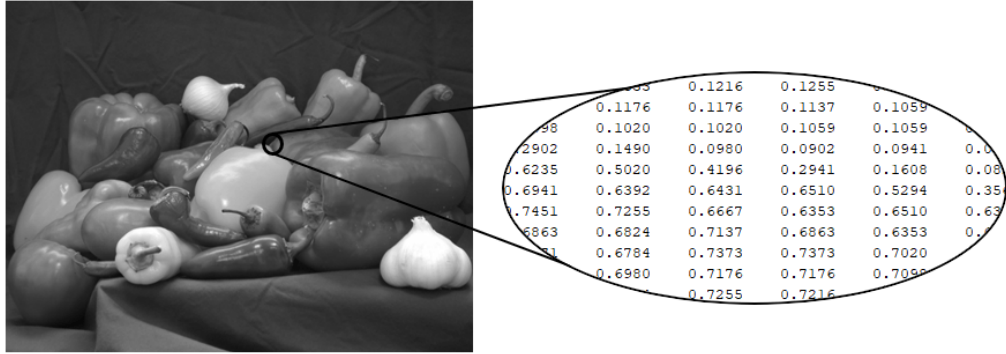
Fig. 3. 10 Grayscale image processing. Image reproduced from Mathworks Image Processing Toolbox, accessed 2022

3.3.7 FTM Image-Based Fiber Orientation Calculator

An Image-Based Fiber Orientation Calculator using Fourier Transform run using an algorithm was used in the orientation analysis of fiber network images. *Matlab ver. R2020b (MathWorks)* was used to run the Image-Based Fiber Orientation Calculator. First, the image was cropped into square size and exported as an 8-bit image. The pre-processed image was read using the calculator. The network orientation tensor, Ω was calculated using **Eq. 3.1**:

$$\Omega = \frac{\sum l_i \begin{bmatrix} cos^2\theta_i & cos\theta_i sin\theta_i \\ cos\theta_i sin\theta_i & cos^2\theta_i \end{bmatrix}}{l_i} \tag{3.1}$$

where l_i is the length of the fiber segment i. The sum accounts for all the fibers in the network. The orientation distribution represented using polar graph was determined by summing the length of each fiber oriented between 0° and 180° at 1° intervals. From the tensor orientation, the eigenvalues and eigenvectors were computed, providing the magnitude and direction of the principal axes. The anisotropy index, α is finally calculated using **Eq. 3.2**.

61

$$\alpha = 1 - \left(\frac{\lambda_1}{\lambda_2}\right) \tag{3.2}$$

Here we will refer to the anisotropy index, α as the alignment factor (AF), to avoid confusion. The eigenvalues are λ_1, λ_2 where $\lambda_1 \leq \lambda_2$. A perfectly random network or anisotropic network has a an α value of zero ($\alpha = 0$, perfectly random). On the other hand, a completely aligned network has a maximum value of 1 ($\alpha =$ 1, perfectly aligned).

3.3.8 SEM Test Image: Alignment Factor (AF) Calculation

The degree of alignment (AF) of the BNNT film fabricated using purified and dispersed system in EC system (Chapter 2) was used as a test image using the alignment calculator previously discussed. The raw SEM image is preprocessed by removing the scale bar and other part of the image that can contribute to noise. Two square images, cropped from the raw image are used in determining the AF, α of the BNNT film (**Fig. 3.11**) to ensure that all the BNNT tubes are accounted.
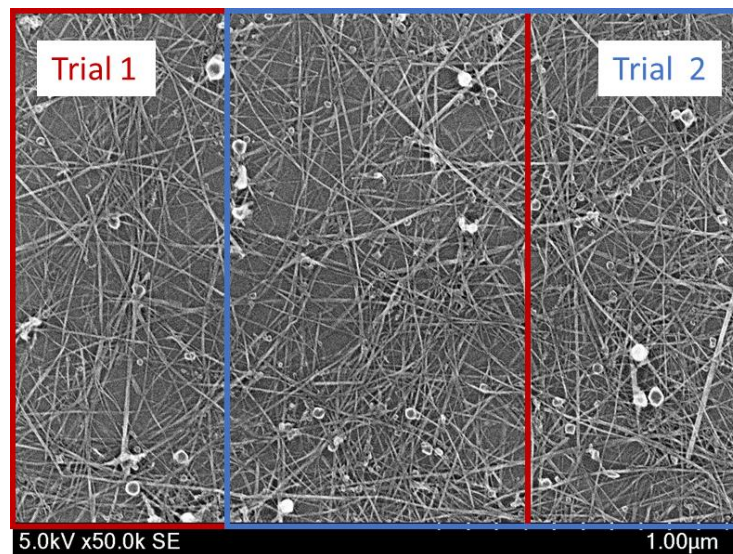
3.3.9 Alignment Factor (AF) Calculation Results: SEM Test Image

The BNNT in the films fabricated using the dispersion system previously developed is randomly oriented with 8.96% degree of alignment (**Table 3.1**). **Fig. 3.12 and 3.13** show the imported image with adjusted contrast and the corresponding intensity scale bar on the right (A), the vectors summarizing the magnitude and directions of the nanotubes (B), the FFT image (C), and the polar plot showing the distribution of the BNNT in the film (D), for Trials 1 and 2, respectively.

Table 3.1. Orientation matrices (Ω), Eigenvalues (λ_1, λ_2) and degree of alignment (α) of BNNT-EC film

	Trial 1		Trial 2	
Ω	0.4758	-0.0042	0.4795	-0.0088
	-0.0042	0.5242	-0.0088	0.5205
λ_1, λ_2	0.4754, 0.5246		0.4777, 0.5223	
α	0.0937		0.0854	
α_{mean} : 0.0896				
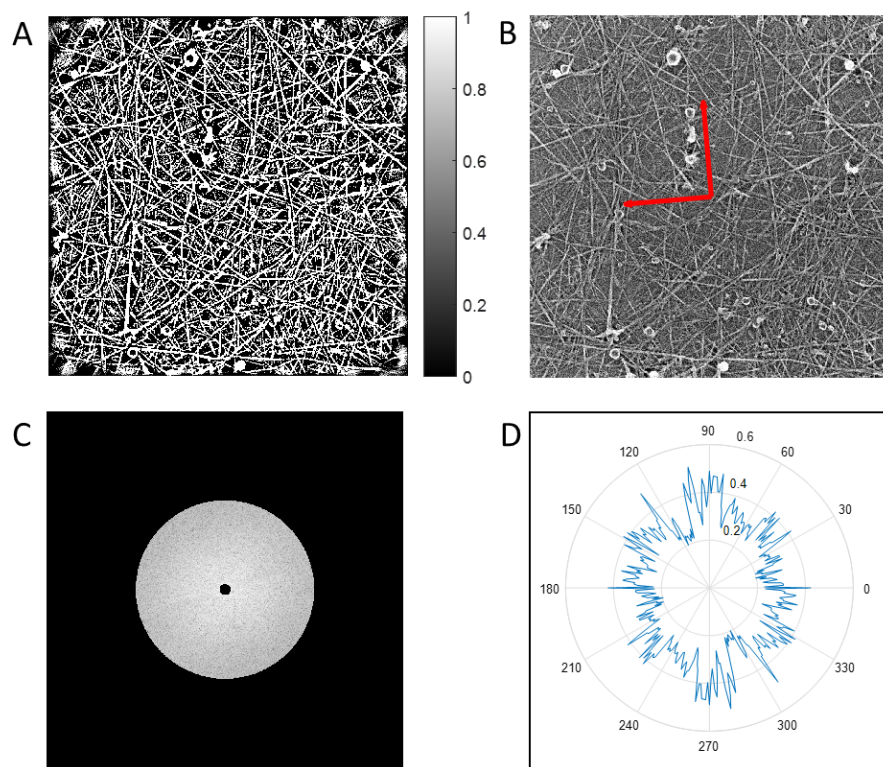
Fig. 3. 12 Pre-processing or raw SEM image for alignment quantification (Trial 1)
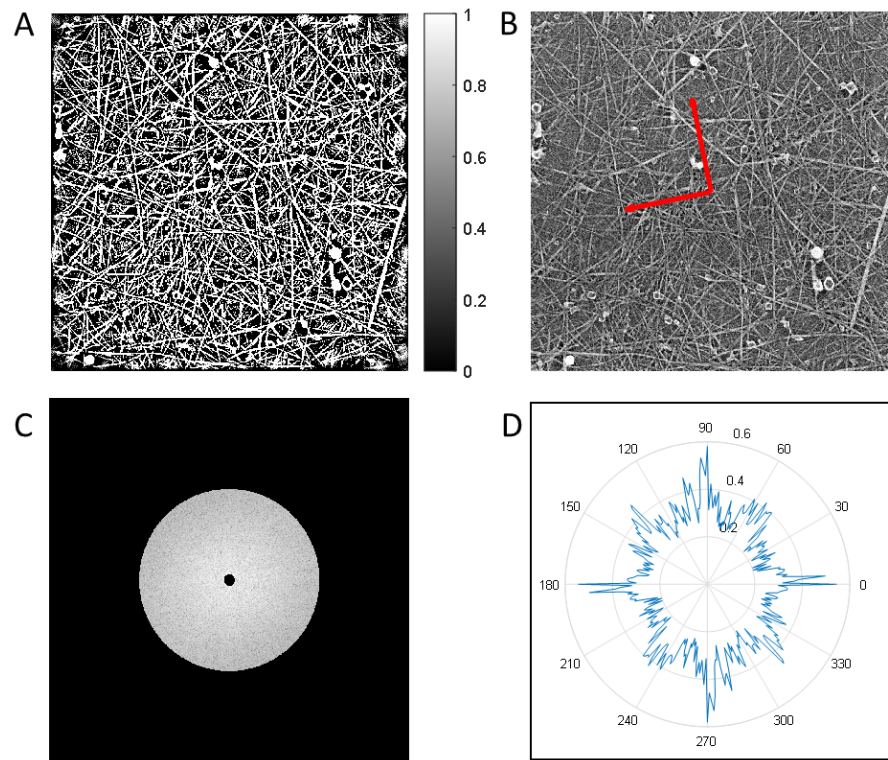
Fig. 3. 13 Pre-processing or raw SEM image for alignment quantification (Trial 2)

3.3.10 Relationship of Alignment and Film Area

We established a relationship between the film size and the alignment of

the BNNT. At least 10 images of different sizes or field of view at different areas

of the film were acquired, preprocessed, and use as input to the alignment

calculator. Representative results are shown in **Fig. 3.14**. The calculated AF were

tabulated and summarized in **Table 3.2.**

A: 1936 μm²

B: 310 μm²

C: 77 μm²

D: 19 μm²

E: 5 μm²

F: 3 μm²

G: 1 μm²
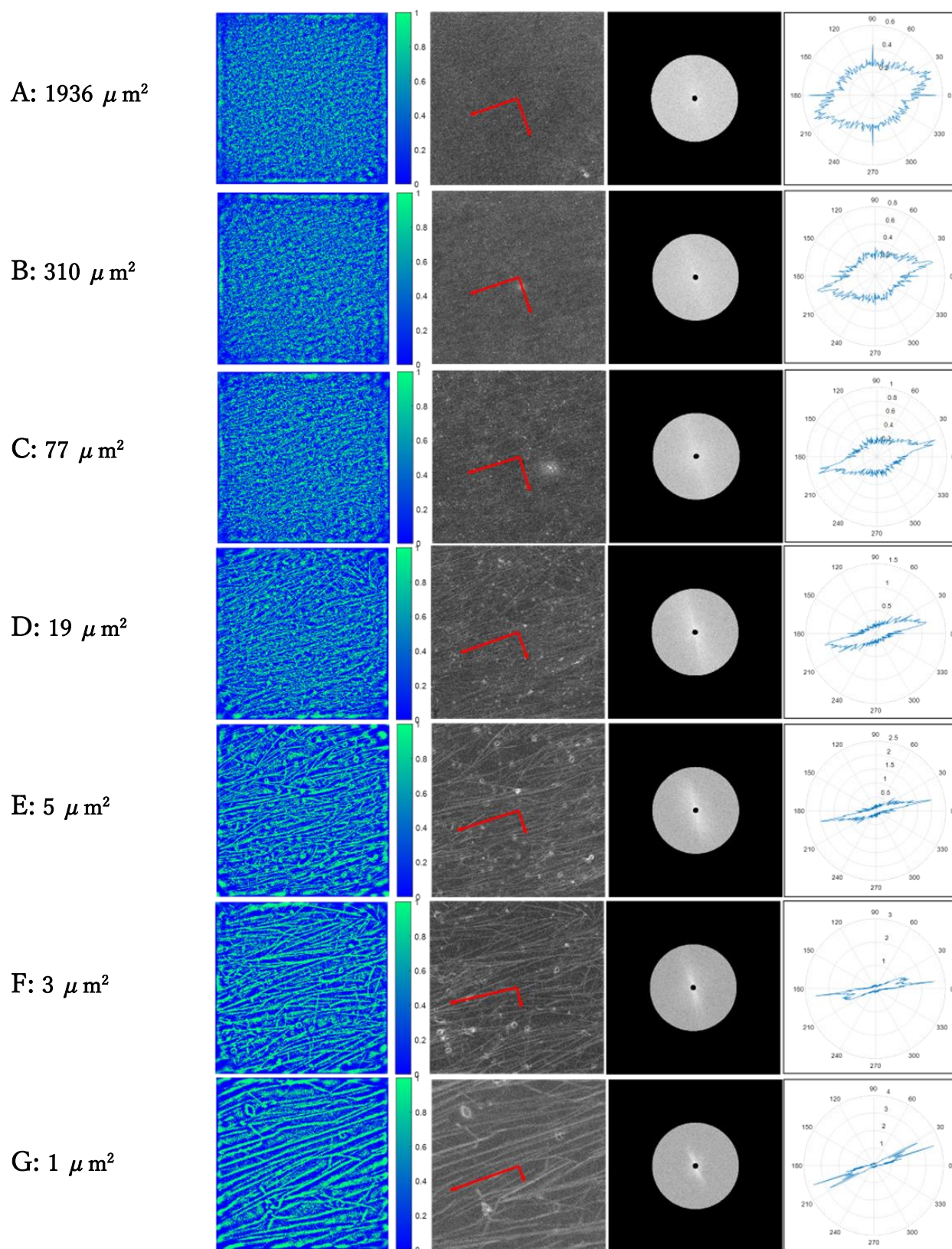
Fig. 3. 14 Alignment quantification at increasing magnification of the BNNT film, i.e., decreasing the area or field of view. Ten (10) SEM images were pre-processed and run per area for reliability.

3.3.11 Degree of alignment and size of the film

Table 2.2. Estimation of alignment at increasing size area of the BNNT film

Area (μm²)	Alignment Factor (AF)						
	1	3	5	19	77	310	1936
1	0.73	0.69	0.62	0.46	0.35	0.28	0.22
2	0.78	0.76	0.50	0.55	0.44	0.31	0.22
3	0.75	0.61	0.60	0.53	0.43	0.30	0.21
4	0.73	0.57	0.74	0.53	0.43	0.30	0.14
5	0.78	0.70	0.64	0.44	0.40	0.25	0.23
6	0.69	0.75	0.56	0.58	0.47	0.34	0.27
7	0.76	0.65	0.67	0.52	0.43	0.35	0.15
8	0.65	0.66	0.67	0.59	0.49	0.35	0.28
9	0.70	0.69	0.61	0.45	0.31	0.23	0.21
10	0.69	0.67	0.68	0.61	0.42	0.29	0.21
Mean	0.73	0.68	0.63	0.53	0.42	0.30	0.21

(Left vertical label: Trial / Run per indicated area)

The calculated AF increases as the size of the film is decreased, i.e., the field of view of the SEM is increased. Understandably, as we zoom in further up to a single 1D nanotube, we would expect an alignment approaching to unity.

$$y = -0.1621x + 0.7309$$
$$R^2 = 0.9888$$
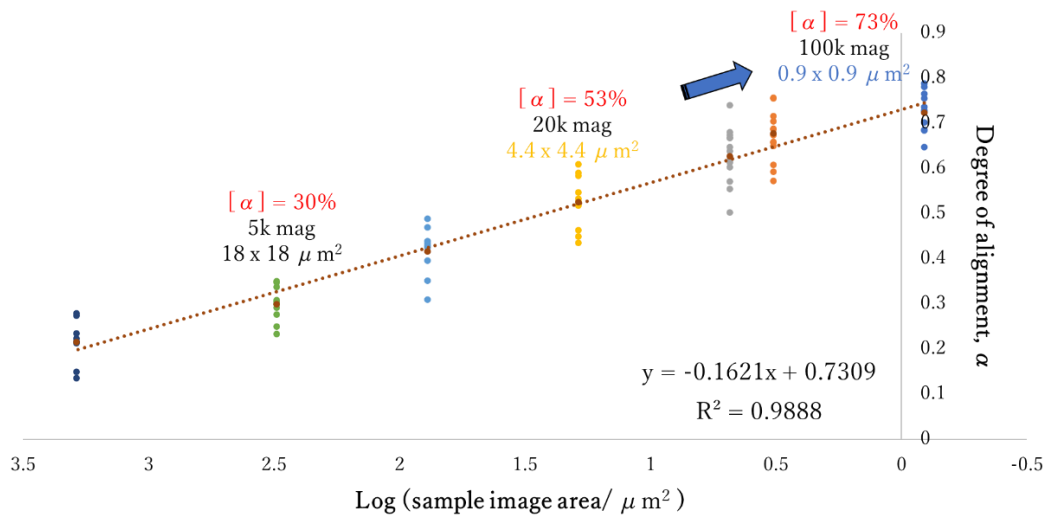
Fig. 3. 15 Logarithmic relationship of the size and alignment

The AF and sample image area follows a linear logarithmic relationship as shown in **Fig. 3.15**. The arrays of highly aligned BNNTs contained in 1x1 μ m^2 film size has a mean of 0.73 AF and a maximum AF of 0.78 or 78%. Increasing the film size by 2000 times (2000x) resulted to 0.21 AF. Recalling the randomly ordered BNNT film using EC as surfactant, the calculated AF is only about 0.0896 or 8.96%, for 1x1 μ m^2 (**Fig. 3.11-3.13**). Hence, we can expect highly aligned arrays of BNNT contained in a uniformly deposited films even in the microscale level.

3.3.12 Alignment of multi-layer deposited BNNT films

We have demonstrated a simple method of depositing uniform monolayer of BNNT by controlling the concentration of the surfactant used, PVB. Here, we developed multi-layers of BNNT by carefully dropping the same amount of dispersion exactly on top of the previously cast films, shown in **Fig. 3.16**.
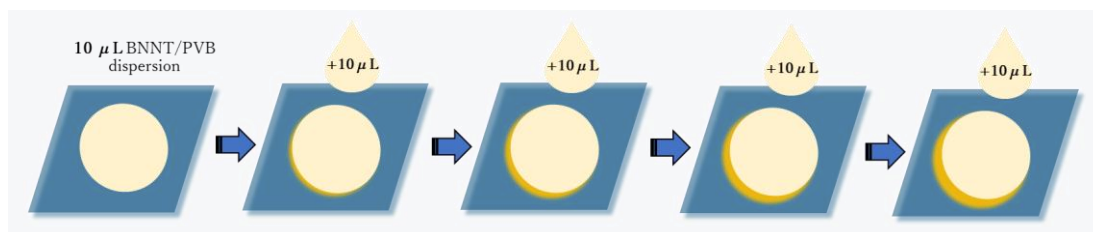
Fig. 3. 16 Repeated casting and drying of BNNT/PVB dispersion in Si substrate to deposit layer of thin film on top of previously deposited layers. [300 ºC, 5 ºC/min, 8 hours]

The calculated AF after depositing the 2nd layer has been reduced by about 20%, from 70% AF to 50% AF. However, the degree of alignment is kept constant until the 5th layer of drop cast BNNT. **Table 3.3** summarizes the calculated AF at different layers of deposited BNNT. The 2nd until the 5th layer has almost the same

AF depicted in **Fig. 3.17**, hence we can expect high order alignment even with multi-layer deposited BNNT films.

Table 3.3. Alignment quantification per layer of deposited BNNT films

	Layers of BNNT film				
Trial	1st	2nd	3rd	4th	5th
1	0.74	0.60	0.43	0.51	0.52
2	0.69	0.35	0.31	0.45	0.46
3	0.63	0.58	0.42	0.37	0.49
4	0.72	0.49	0.47	0.45	0.60
5	0.66	0.44	0.35	0.53	0.57
Mean	**0.72**	**0.48**	**0.43**	**0.48**	**0.53**
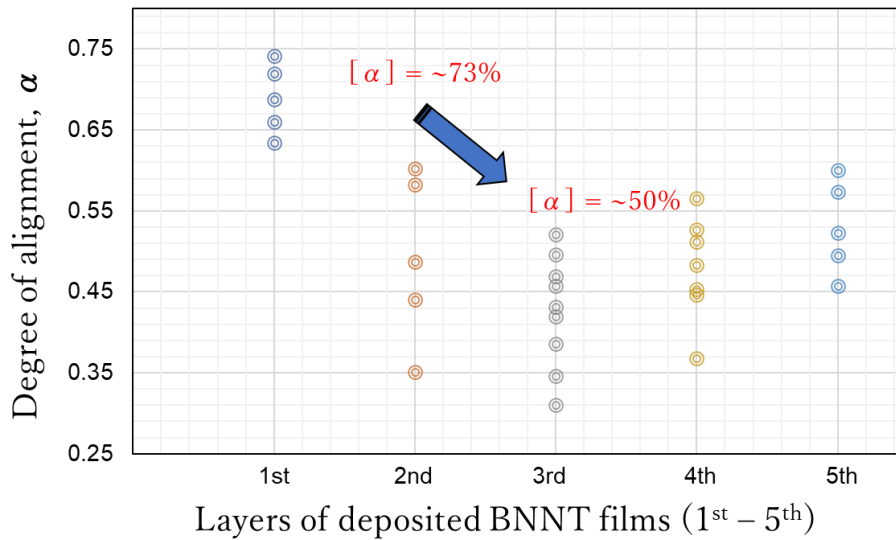
Fig. 3. 17 Alignment of multi-layered BNNT films. 1.8 x 1.8 μm^2 sample area was used in the calculation of the alignment factor

3.3.13 Mechanical scratches and alignment

Fig. 3.18A outlines the procedure used to introduce scratches or gratings in the substrate. After brushing with a membrane filfter containing cellulose, the gratings (Fig. 3.18C) was successfully drawn in the cleaned and smooth surface (Fig. 3.18B).
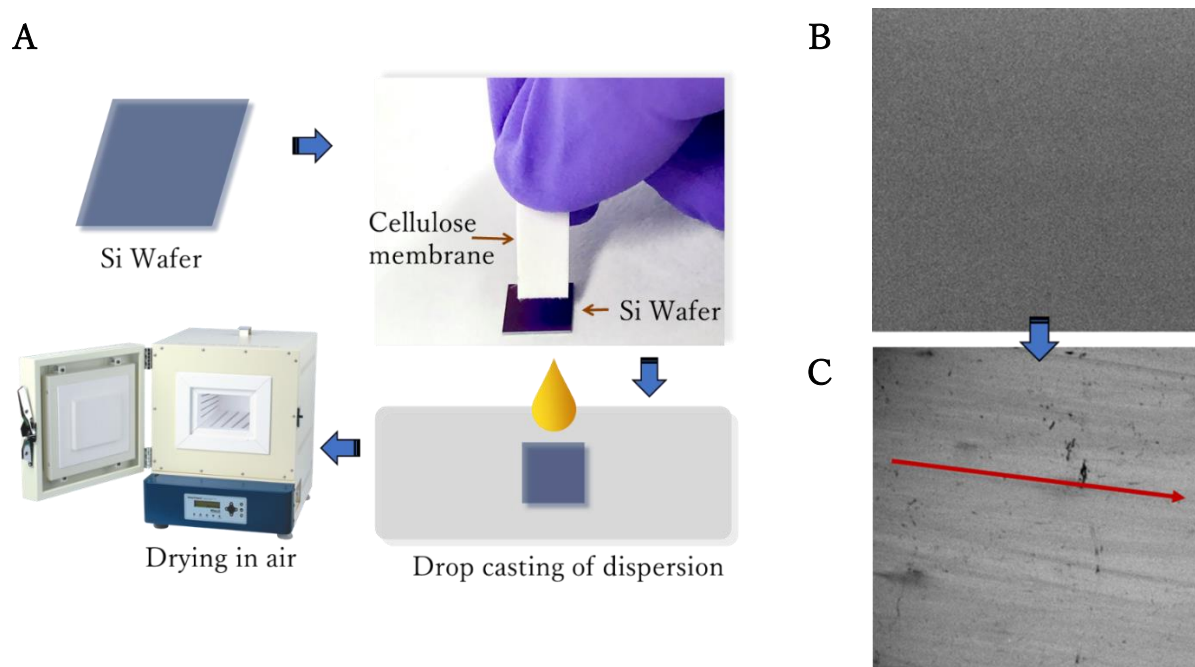
Fig. 3. 18 Mechanical brushing via soft-friction transfer (A) of cleaned silica wafer (B) introducing aligned gratings in the substrate (C). The direction of the gratings is indicated by the arrow (→)

After mechanical brushing, we observed some improvement in the alignment of the BNNT as indicated by the long red arrow (→) in Fig. 3.19B. The calculated AF has been improved by about 20% compared to the non-brushed surface in Table 3.4. We further confirmed whether such improvement is due to

the cellulose transferred on the substrate or the gratings due to mechanical scratching by washing the pre-scratched surface before the deposition process. Our results suggest the minimal effect of cellulosic residues on the substrate to the alignment, rather such significant improvement can be attributed to the gratings that can served as template for the BNNT/PVB assemblies.
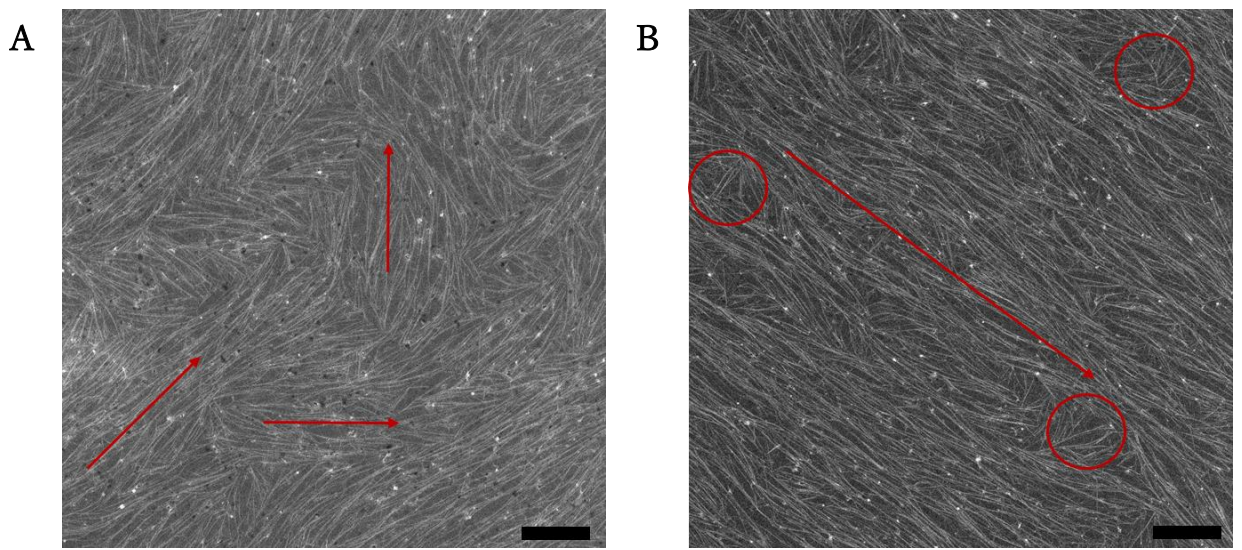
Fig. 3. 19 SEM of deposited BNNT films before (A) and after mechanical brushing (B) of the substrate used. [**Scale: 1 μ m**]

Table 3.4. Enhanced alignment after mechanical brushing

Substrate	Trial	Eigenvalues: λ_1, λ_2	AF	Ave. AF
non-brushed	1	0.2514, 0.7486	0.6642	0.6833
	2	0.2293, 0.7707	0.7025	
brushed	1	0.1280, 0.8720	0.8532	0.8419
	2	0.1448, 0.8552	0.8307	
brushed, washed	1	0.1471, 0.8529	0.8275	0.8192
	2	0.1590, 0.8410	0.8109	

The significant improvement in the alignment of the BNNT due to the control of various factors such as the type and concentrations of the polymer used, surface treatment, and multi-layer deposition of films are best depicted in **Fig. 3.20.**
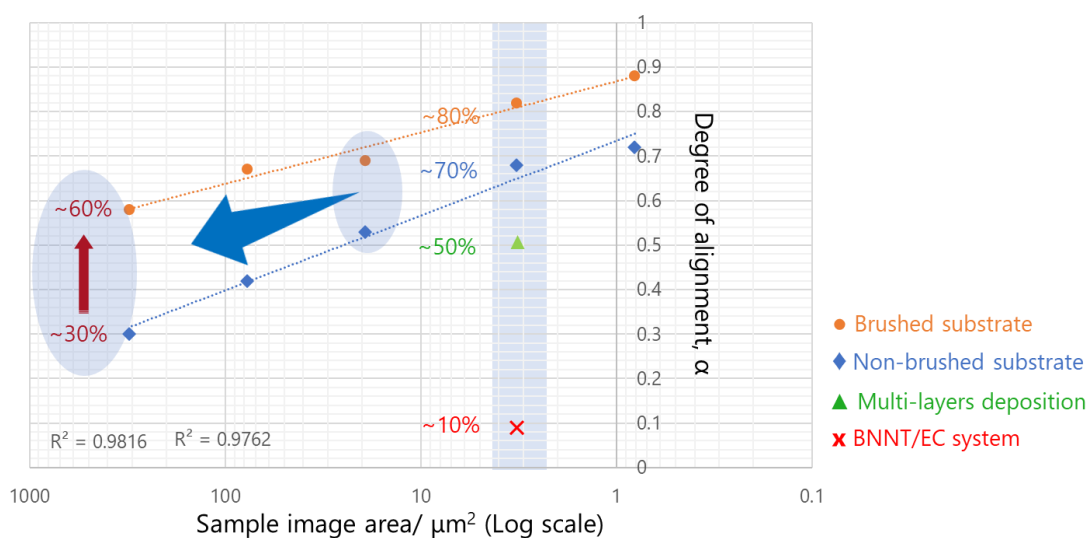
Fig. 3. 20 Calculated alignment after mechanical brushing; comparison alignment factors for various BNNT films prepared.

The blue plot corresponding to mono-layer deposits of BNNTs over a non-brushed substrate shows a linear logarithmic relationship of the alignment and the film size. This direct relationship was also observed after mechanically brushing the substrate, shown in the orange plot. Surprisingly, a decrease in the slope of the plot upon substrate treatment was observed indicating a significant improvement in the calculated alignment of BNNT on larger size of the film.

Ideally, the slope of the plot will approach zero for a globally aligned BNNTs in the film, *i.e.* all the BNNTs in the film are aligned in one direction. Therefore, such linear logarithmic relationship between the size of the film and the alignment of BNNT, which we have established for the first time from this study would be significant to attain globally aligned BNNTs.

3.4 Conclusion

In summary, we have examined the fabrication of BNNT films drop cast and dried over a substrate. The PVB surfactant introduced in the system produced a stable colloidal dispersion of BNNT. More importantly, our results revealed the formation of uniform patterns containing networks or assemblies of the 1D system.

At low surfactant concentrations, ring-shaped deposits in the pheripheries were formed. At intermediate surfactant concentrations, the patterns of the deposited dispersion were homogeneous, however, at higher concentrations, more concentric rings from the center to the edge of the deposit are formed.

Moreover, the uniformly deposited films contain arrays of aligned BNNTs. A random to ordered orientation from the center to the edge of the film was evident from the SEM images. Our observation suggests that using the surfactant, depinning of the contact line helped in such uniform patterns.

The alignment of the BNNT was also quantified using an alignment calculator, comparing the improvement in the orientation of BNNT using PVB. The alignment is also retained even at multi-layered BNNT film deposits. More importantly, we have reliably established a linear logarithmic relationship of the

alignment of BNNT in various sizes of films, via image-based alignment quantification technique. To date, such relatioship have not yet been established or achieved using other alignment quantification methods. Our methods would be useful toward uniform deposition of highly aligned BNNTs to advance their applications.

Chapter 4

Conclusion

For the past 27 years since the first successful synthesis of boron nitride nanotubes (BNNTs), efforts have increased to utilize them for various novel applications. BNNTs are structurally analogous to carbon nanotubes (CNTs), possessing excellent mechanical properties but uniquely owning a different set of multifunctional characteristics such as higher thermal stability, a wider band gap making them transparent in the visible region, piezoelectric property, and high neutron absorption. Especially in the past few years, success in producing a large amount of BNNTs has sparked researchers to explore their applications in the aerospace, biomedical, energy storage systems, and semiconductor industries.

As newly emerging nanomaterials, the development of BNNTs still lags behind their well-studied CNTs counterpart. However, with the recent attention, we are yet to expect an exciting future for BNNTs. Hence, we are glad to share the results of this thesis

in an attempt to contribute to the solution and solid-based processing technologies for BNNTs.

We first discussed a brief background on the current BNNT production and purification issues in the first chapter. Successful methods of producing gram-amount of BNNT at a faster rate have been achieved; however, the presence of impurities has remained a challenge. The successful purification scheme was developed using a cost-effective and more practical approach discussed. Using a nontoxic, cheaper, and widely available ethyl cellulose (EC) as a dispersant, simultaneous purification, and dispersion of BNNT bulk-produced via induction plasma-torch method was achieved. The stable dispersions using different solvents were also designed due to the wider solubility of EC at various solvents.

Translated into a solid-state system, we can make use and take advantage of the excellent properties of BNNTs. Therefore, the dispersion system we previously designed was used to fabricate BNNT films using a simple deposition method. Evaporative-driven structure formation was discussed, modulating mainly a coffee-ring (CR) pattern typically observed when a dispersion of suspended particles is drop-cast and left dried over a substrate. The use of PVB in our system assisted in the modulation of the CR pattern, where we successfully obtained a uniform deposit of the BNNT film in the substrate. High-resolution scanning electron microscopy (SEM) was used to investigate the nano-assemblies in the film revealing hierarchical assemblies or alignment of BNNT in the deposited film.

Further, we employed SEM image analysis to quantify the degree of alignment in the film. From the results, the alignment of BNNT is achievable even for multi-layered deposited film. Gratings or templated substrate can also enhance alignment. From the

randomly deposited BNNT with 8.96% alignment factor (AF) using EC system, we succeeded in attaining 78% AF using PVB system in the highly aligned arrays of BNNTs contained in 1x1 $\mu\,\text{m}^2$ film. The established linear logarithmic relationship would be helpful towards the global alignment of BNNTs in film.

Recommendations and Prospects

This research has successfully developed a practical approach to purify BNNTs enabling uniform and stable colloidal dispersions of BNNT. A wider range of solvents can be used in the dispersion depending on the solubility of the dispersant used. Here we used two types of non-aromatic polymer: ethyl cellulose (EC) and polyvinyl butyral (PVB). To increase more the dispersibility data of BNNT, more dispersant systems can be investigated using various polymer and solvent systems. Other characterizations, including but not limited to the optical absorption of the dispersion, can also be done to evaluate their properties. These data would be helpful in the future design of the dispersion of BNNTs via Machine Learning approach, which in turn would speed up the processing and application of BNNTs.

In the second part of this research, higher control of the alignment can be possibly achieved by in-depth studying, quantifying, and controlling the side functional groups present in PVB. In the future, we can perhaps design or synthesize a polymer to fully control these side groups that can significantly align BNNTs. Moreover, the effect of other factors such as the use of other substrate and substrate treatment, on the alignment of BNNTs could be studied. Other alignment quantification techniques like Raman

spectroscopy could also be considered to possibly obtain a correlation between the image analysis we employed in this work and other available methods.

Lastly, we hope that the attempts in this research: the development of the solution and solid-based processing technologies for BNNTs, would advance their applications. Therefore, the actual application of the fabricated films, such as BNNT-coated substrates, can be continued using the results of this work. Self-standing transparent and flexible BNNT films can also be fabricated to characterize their mechanical property, thermal stability, and piezoelectricity.

References

1.	Ciofani, G., Raffa, V., Menciassi, A. & Cuschieri, A. Boron nitride nanotubes: An innovative tool for nanomedicine. *Nano Today* **4**, 8–10 (2009).

2.	Kim, H. S. *et al.* Boron nitride nanotube-based separator for high-performance lithium-sulfur batteries. *Nanomaterials* **12**, (2022).

3.	Lenin, A. *et al.* Hybrid Ni-boron nitride nanotube magnetic semiconductor - A new material for spintronics. *ACS Omega* **5**, 20014–20020 (2020).

4.	Langley Research Center. LASA web.pdf. *NASA Research News* https://www.nasa.gov/centers/langley/news/researchernews/rn_BNNT.html (2022).

5.	Kim, J. H., Pham, T. V., Hwang, J. H., Kim, C. S. & Kim, M. J. Boron nitride nanotubes: synthesis and applications. *Nano Converg.* **5**, (2018).

6.	Golberg, D. *et al.* Boron Nitride Nanotubes and Nanosheets. *ACS Nano* **4**, 2979–2993 (2010).

7.	Golberg, D., Bando, Y., Tang, C. C. & Zhi, C. Y. Boron Nitride Nanotubes. *Adv. Mater.* **19**, 2413–2432 (2007).

8.	Chang, C. W. *et al.* Isotope effect on the thermal conductivity of boron nitride nanotubes. *Phys. Rev. Lett.* **97**, 1–4 (2006).

9. Stewart, D. A., Savic, I. & Mingo, N. First-principles calculation of the isotope effect on boron nitride nanotube thermal conductivity. *Nano Lett.* **9**, 81–84 (2009).

10. Arenal, R., Wang, M.-S., Xu, Z., Loiseau, A. & Golberg, D. Young modulus, mechanical and electrical properties of isolated individual and bundled single-walled boron nitride nanotubes. *Nanotechnology* **22**, 265704 (2011).

11. Suryavanshi, A. P., Yu, M. F., Wen, J., Tang, C. & Bando, Y. Elastic modulus and resonance behavior of boron nitride nanotubes. *Appl. Phys. Lett.* **84**, 2527–2529 (2004).

12. Chopra, N. G. & Zettl, A. Measurement of the elastic modulus of a multi-wall boron nitride nanotube. *Solid State Commun.* **105**, 297–300 (1998).

13. Lauret, J. S. *et al.* Optical transitions in single-wall boron nitride nanotubes. *Phys. Rev. Lett.* **94**, 1–4 (2005).

14. Zhi, C., Bando, Y., Tang, C. & Golberg, D. Boron nitride nanotubes. *Mater. Sci. Eng. R Reports* **70**, 92–111 (2010).

15. Blase, X., Rubio, A., Louie, S. G. & Cohen, M. L. Stability and Band Gap Constancy of Boron Nitride Nanotubes. *Europhys. Lett.* **28**, 335–340 (1994).

16. Cohen, M. L. & Zettl, A. The physics of boron nitride nanotubes. *Phys. Today* **63**, 34–38 (2010).

17.   Nakhmanson, S. M., Calzolari, A., Meunier, V., Bernholc, J. & Nardelli, M. B. Spontaneous polarization and piezoelectricity in boron nitride nanotubes. *Phys. Rev. B - Condens. Matter Mater. Phys.* **67**, 1–6 (2003).

18.   Dai, Y., Guo, W., Zhang, Z., Zhou, B. & Tang, C. Electric-field-induced deformation in boron nitride nanotubes. *J. Phys. D. Appl. Phys.* **42**, (2009).

19.   Ban, C., Jiang, X., Li, L. & Liu, X. The piezoelectric and dielectric properties of flexible, nanoporous, self-assembled boron nitride nanotube thin films. *J. Mater. Sci.* **54**, 14074–14084 (2019).

20.   Yamakov, V., Park, C., Ho, J., Wise, K. E. & Fay, C. Piezoelectric molecular dynamics model for boron nitride nanotubes. *Comput. Mater. Sci.* **95**, 362–370 (2014).

21.   Yamakov, V. *et al.* Piezoelectric and elastic properties of multiwall boron-nitride nanotubes and their fibers: A molecular dynamics study. *Comput. Mater. Sci.* **135**, 29–42 (2017).

22.   Tamayo, P. *et al.* Review on neutron-absorbing fillers. in *Micro and Nanostructured Composite Materials for Neutron Shielding Applications* 25–52 (Elsevier, 2020). doi:10.1016/B978-0-12-819459-1.00002-7.

23.   Chopra, N. *et al.* Boron nitride nanotubes. *Science (80-.).* **269**, 967–967 (1995).

24. Kim, J. *et al.* Synthesis and growth of boron nitride nanotubes by a ball milling-annealing process. *Acta Mater.* **59**, 2807–2813 (2011).

25. Lourie, O. R. *et al.* CVD growth of boron nitride nanotubes. *Chem. Mater.* **12**, 1808–1810 (2000).

26. Ahmad, P., Khandaker, M. U., Khan, Z. R. & Amin, Y. M. Synthesis of boron nitride nanotubes via chemical vapour deposition: A comprehensive review. *RSC Adv.* **5**, 35116–35137 (2015).

27. Yu, D. P. *et al.* Synthesis of boron nitride nanotubes by means of excimer laser ablation at high temperature. *Appl. Phys. Lett.* **72**, 1966–1968 (1998).

28. Fathalizadeh, A., Pham, T., Mickelson, W. & Zettl, A. Scaled synthesis of boron nitride nanotubes, nanoribbons, and nanococoons using direct feedstock injection into an extended-pressure, inductively-coupled thermal plasma. *Nano Lett.* **14**, 4881–4886 (2014).

29. Mi, C. S. *et al.* Synthesis of Boron Nitride Nanotubes via inductively Coupled thermal Plasma process Catalyzed by Solid-state ammonium Chloride. *J. Korean Powder Metall. Inst.* **25**, 120–125 (2018).

30. Lee, C. M., Choi, S. I., Choi, S. S. & Hong, S. H. Synthesis of boron nitride nanotubes by arc-jet plasma. *Curr. Appl. Phys.* **6**, 166–170 (2006).

31. Kim, K. S. *et al.* Hydrogen-catalyzed, pilot-scale production of small-diameter boron nitride nanotubes and their macroscopic assemblies. *ACS Nano* **8**, 6211–6220 (2014).

32. Harrison, H. *et al.* Quantification of hexagonal boron nitride impurities in boron nitride nanotubes via FTIR spectroscopy. *Nanoscale Adv.* **1**, 1693–1701 (2019).

33. Cui, Z., Oyer, A. J., Glover, A. J., Schniepp, H. C. & Adamson, D. H. Large scale thermal exfoliation and functionalization of boron nitride. *Small* **10**, 2352–2355 (2014).

34. Torres Castillo, C. S., Bruel, C. & Tavares, J. R. Chemical affinity and dispersibility of boron nitride nanotubes. *Nanoscale Adv.* **2**, 2497–2506 (2020).

35. Chen, H., Chen, Y., Yu, J. & Williams, J. S. Purification of boron nitride nanotubes. *Chem. Phys. Lett.* **425**, 315–319 (2006).

36. Smith McWilliams, A. D. *et al.* Surfactant-assisted individualization and dispersion of boron nitride nanotubes. *Nanoscale Adv.* **1**, 1096–1103 (2019).

37. Gao, Z., Zhi, C., Bando, Y., Golberg, D. & Serizawa, T. Isolation of individual boron nitride nanotubes via peptide wrapping. *J. Am. Chem. Soc.* **132**, 4976–4977 (2010).

38. Shin, H. *et al.* Covalent Functionalization of Boron Nitride Nanotubes via

Reduction Chemistry. *ACS Nano* **9**, 12573–12582 (2015).

39. Gao, Z., Zhi, C., Bando, Y., Golberg, D. & Serizawa, T. Noncovalent functionalization of disentangled boron nitride nanotubes with flavin mononucleotides for strong and stable visible-light emission in aqueous solution. *ACS Appl. Mater. Interfaces* **3**, 627–632 (2011).

40. Lee, C. H., Zhang, D. & Yap, Y. K. Functionalization, Dispersion, and Cutting of Boron Nitride Nanotubes in Water. *J. Phys. Chem. C* **116**, 1798–1804 (2012).

41. Velayudham, S. *et al.* Noncovalent functionalization of boron nitride nanotubes with poly(p-phenylene-ethynylene)s and polythiophene. *ACS Appl. Mater. Interfaces* **2**, 104–110 (2010).

42. Yu, J., Chen, Y. & Cheng, B. M. Dispersion of boron nitride nanotubes in aqueous solution with the help of ionic surfactants. *Solid State Commun.* **149**, 763–766 (2009).

43. Zhi, C. *et al.* Perfectly Dissolved Boron Nitride Nanotubes Due to Polymer Wrapping. *J. Am. Chem. Soc.* **127**, 15996–15997 (2005).

44. Amin, M. S. *et al.* High-purity boron nitride nanotubes via high-yield hydrocarbon solvent processing. *Chem. Mater.* **31**, 8351–8357 (2019).

45. Marincel, D. M. *et al.* Scalable Purification of Boron Nitride Nanotubes via Wet

Thermal Etching. *Chem. Mater.* **31**, 1520–1527 (2019).

46.   Lee, C. H. *et al.* Boron nitride nanotubes: Recent advances in their synthesis,

       functionalization, and applications. *Molecules* **21**, (2016).

47.   Rekhi, G. S. & Jambhekar, S. S. Ethylcellulose - a polymer review. *Drug Dev. Ind.*
       Pharm. **21**, 61–77 (1995).

48.   Wasilewska, K. & Winnicka, K. Ethylcellulose-a pharmaceutical excipient with

       multidirectional application in drug dosage forms development. *Materials (Basel).*
       12, (2019).

49.   Adeleke, O. A. Premium ethylcellulose polymer based architectures at work in drug

       delivery. *Int. J. Pharm. X* **1**, 100023 (2019).

50.   De los Reyes, F. D., Fujieda, T., Takeuchi, A., Kawai, T. & Nonoguchi, Y. Isolation

       of exfoliated boron nitride nanotubes via ethyl cellulose wrapping. *Nano Sel.*
       nano.202000265 (2021) doi:10.1002/nano.202000265.

51.   Kim, D. *et al.* Sonication-assisted alcoholysis of boron nitride nanotubes for their

       sidewalls chemical peeling. *Chem. Commun.* **51**, 7104–7107 (2015).

52.   Lee, C. H., Wang, J., Kayatsha, V. K., Huang, J. Y. & Yap, Y. K. Effective growth

       of boron nitride nanotubes by thermal chemical vapor deposition. *Nanotechnology*
       19, (2008).

53. Zhao, L. *et al.* High-temperature dielectric paper with high thermal conductivity and mechanical strength by engineering the aramid nanofibers and boron nitride nanotubes. *Mater. Des.* **210**, 110124 (2021).

54. Long, F. & Zhou, B. Reinforced Boron Carbide Ceramics. 187–194 (2021).

55. Cong, Z. & Lee, S. Study of mechanical behavior of BNNT-reinforced aluminum composites using molecular dynamics simulations. *Compos. Struct.* **194**, 80–86 (2018).

56. Khoury, J. F., Vitale, J. C., Larson, T. L. & Ao, G. Boron nitride nanotubes enhance mechanical properties of fibers from nanotube/polyvinyl alcohol dispersions. *Nanoscale Adv.* **4**, 77–86 (2022).

57. Goh, P. S., Ismail, A. F. & Ng, B. C. Directional alignment of carbon nanotubes in polymer matrices: Contemporary approaches and future advances. *Compos. Part A Appl. Sci. Manuf.* **56**, 103–126 (2014).

58. Hussain, F., Hojjati, M., Okamoto, M. & Gorga, R. E. Review article: Polymer-matrix nanocomposites, processing, manufacturing, and application: An overview. *J. Compos. Mater.* **40**, 1511–1575 (2006).

59. Xie, X. L., Mai, Y. W. & Zhou, X. P. Dispersion and alignment of carbon nanotubes in polymer matrix: A review. *Mater. Sci. Eng. R Reports* **49**, 89–112 (2005).

60. Liu, L. *et al.* Aligned, high-density semiconducting carbon nanotube arrays for high-performance electronics. *Science (80-.).* **368**, 850–856 (2020).

61. De Heer, W. A. *et al.* Aligned carbon nanotube films: Production and optical and electronic properties. *Science (80-.).* **268**, 845–847 (1995).

62. Akhtar, I. & Chang, S. H. *Highly aligned carbon nanotubes and their sensor applications. Nanoscale* vol. 12 (2020).

63. Belkerk, B. E. *et al.* Thermal conductivity of vertically aligned boron nitride nanotubes. *Appl. Phys. Express* **9**, (2016).

64. Kang, J. H. *et al.* Multifunctional Electroactive Nanocomposites Based on Piezoelectric Boron Nitride Nanotubes. *ACS Nano* **9**, 11942–11950 (2015).

65. Wang, Z. *et al.* Alignment of boron nitride nanofibers in epoxy composite films for thermal conductivity and dielectric breakdown strength improvement. *Nanomaterials* **8**, 1–14 (2018).

66. Terao, T. *et al.* Alignment of boron nitride nanotubes in polymeric composite films for thermal conductivity improvement. *J. Phys. Chem. C* **114**, 4340–4344 (2010).

67. Mampallil, D. & Eral, H. B. A review on suppression and utilization of the coffee-ring effect. *Adv. Colloid Interface Sci.* **252**, 38–54 (2018).

68. Deegan, R. D. *et al.* Capillary flow as the cause of ring stains from dried liquid

drops. *Nature* **389**, 827–829 (1997).

69.   Deegan, R. D. *et al.* Contact line deposits in an evaporating drop. *Phys. Rev. E -*

Stat. Physics, Plasmas, Fluids, Relat. Interdiscip. Top. **62**, 756–765 (2000).

70.   Park, J. & Moon, J. Control of colloidal particle deposit patterns within picoliter

droplets ejected by ink-jet printing. *Langmuir* **22**, 3506–3513 (2006).

71.   Shimobayashi, S. F., Tsudome, M. & Kurimura, T. Suppression of the coffee-ring

effect by sugar-assisted depinning of contact line. *Sci. Rep.* **8**, 1–9 (2018).

72.   Kajiya, T., Kobayashi, W., Okuzono, T. & Doi, M. Controlling the drying and film

formation processes of polymer solution droplets with addition of small amount of

surfactants. *J. Phys. Chem. B* **113**, 15460–15466 (2009).

73.   Hu, H. & Larson, R. G. Marangoni effect reverses coffee-ring depositions. *J. Phys.*

Chem. B **110**, 7090–7094 (2006).

74.   Anyfantakis, M., Geng, Z., Morel, M., Rudiuk, S. & Baigl, D. Modulation of the

coffee-ring effect in particle/surfactant mixtures: The importance of particle-

interface interactions. *Langmuir* **31**, 4113–4120 (2015).

75.   Seo, C., Jang, D., Chae, J. & Shin, S. Altering the coffee-ring effect by adding a

surfactant-like viscous polymer solution. *Sci. Rep.* **7**, 1–9 (2017).

76.   Weon, B. M. & Je, J. H. Capillary force repels coffee-ring effect. *Phys. Rev. E - Stat.*

Nonlinear, Soft Matter Phys. **82**, 1–4 (2010).

77.   Poulichet, V., Morel, M., Rudiuk, S. & Baigl, D. Liquid-liquid coffee-ring effect. *J. Colloid Interface Sci.* **573**, 370–375 (2020).

78.   Kim, S. J., Kang, K. H., Lee, J., Kang, I. S. & Yoon, B. J. Control of Particle-Deposition Pattern in a Sessile Droplet by Using Radial Electroosmotic Flow. **78**, 5192–5197 (2006).

79.   Phys, A. Effect of superhydrophobic surface morphology on evaporative deposition patterns. **201604**, (2018).

80.   Chaudhuri, S., Nguyen, H., Rangayyan, R. M., Walsh, S. & Frank, C. B. A Fourier Domain Directional Filtering Method for Analysis of Collagen Alignment in Ligaments. *IEEE Trans. Biomed. Eng.* **BME-34**, 509–518 (1987).

81.   Fee, T., Downs, C., Eberhardt, A., Zhou, Y. & Berry, J. Image-based quantification of fiber alignment within electrospun tissue engineering scaffolds is related to mechanical anisotropy. *J. Biomed. Mater. Res. - Part A* **104**, 1680–1686 (2016).

82.   Shehata, N. *et al.* Static-Aligned Piezoelectric Poly (Vinylidene Fluoride) Electrospun Nanofibers/MWCNT Composite Membrane: Facile Method. *Polymers (Basel).* **10**, 965 (2018).

83.   Sander, E. A. & Barocas, V. H. Comparison of 2D fiber network orientation

measurement methods. *J. Biomed. Mater. Res. Part A* **88A**, 322–331 (2009).

84. Imanishi, M., Kajiya, D., Koganezawa, T. & Saitow, K. Uniaxial orientation of P3HT film prepared by soft friction transfer method. *Sci. Rep.* **7**, 5141 (2017).

85. Gao, C. *et al.* Highly improved mechanical performances of polyvinyl butyral through fluorescent carbon dots. *Mater. Lett.* **280**, 128537 (2020).

86. Zieliński, A., Bogdanowicz, R., Ryl, J., Burczyk, L. & Darowicki, K. Local impedance imaging of boron-doped polycrystalline diamond thin films. *Appl. Phys. Lett.* **105**, (2014).

87. Fujita, D. & Sagisaka, K. Active nanocharacterization of nanofunctional materials by scanning tunneling microscopy. *Sci. Technol. Adv. Mater.* **9**, (2008).

88. Ago, H. *et al.* Unidirectional growth of single-walled carbon nanotubes. *J. Am. Chem. Soc.* **130**, 17264–17265 (2008).

89. Walker, J. S. *et al.* Global Alignment of Solution-Based Single-Wall Carbon Nanotube Films via Machine-Vision Controlled Filtration. *Nano Lett.* **19**, 7256–7264 (2019).

90. Cadena, A., Botka, B. & Kamarás, K. Organic molecules encapsulated in single-walled carbon nanotubes. *Oxford Open Mater. Sci.* **1**, 1–16 (2020).

91. Simonsen Ginestra, C. J. *et al.* Liquid crystals of neat boron nitride nanotubes and

their assembly into ordered macroscopic materials. *Nat. Commun.* **13**, 1–8 (2022).

92. Zhou, W. *et al.* Single wall carbon nanotube fibers extruded from super-acid

suspensions: Preferred orientation, electrical, and thermal transport. *J. Appl. Phys.*

95, 649–655 (2004).

93. Arenal, R. *et al.* Raman spectroscopy of single-wall boron nitride nanotubes. *Nano*

Lett. **6**, 1812–1816 (2006).

94. Wirtz, L., Rubio, A., De La Concha, R. & Loiseau, A. Ab initio calculations of the

lattice dynamics of boron nitride nanotubes. *Phys. Rev. B - Condens. Matter Mater.*

Phys. **68**, 1–13 (2003).

Scientific Production

Publications

[1] **De los Reyes FD**, Fujieda T, Takeuchi A, Kawai T, Nonoguchi Y. "Isolation of exfoliated boron nitride nanotubes via ethyl cellulose wrapping". Nano Select. 2021; 2(8), 1517-1524 (Wiley, selected as journal issue cover).

[2] Panis JA, Louis M, Brosseau A, Katao S, **De los Reyes FD**, Nakashima T, Métivier R, Allain C, Kawai T. "Circularly polarized luminescence and circular dichroism of bichromophoric difluoroboron-β-diketonates: inversion and enhanced chirality based on spatial arrangements and self-assembly". Chem. Eur. J. 2022, e202201012.

Patent

[3] 藤枝　正，野々口　斐之，**フロレンシオ　デレン　デロス レイエス (Florencio Delen De los Reyes**)，河合　壮，竹内　明史，"Method of producing boron nitride nanotubes", Patent No. WO2022/102741, (2022).

Conference presentations

[4] **De los Reyes FD**, Fujieda T, Takeuchi A, Kawai T, Nonoguchi Y. Polymer-assisted purification and dispersion of mass-produced boron nitride nanotubes. The International Chemical Congress of Pacific Basin Societies. Dec. 16-21, 2021. (Oral presentation)

[5] **De los Reyes FD**, Louis M, Tsuchie Y, Nonoguchi Y. Kawai T. Highly aligned arrays of boron nitride nanotubes in a coffee-ring pattern: enhancement and image-based quantification studies. The 63rd Fullerenes-Nanotubes-Graphene General Symposium. Aug. 31 – Sept. 2, 2022. (Poster presentation)

Personal page / Acknowledgments

Thank you for reaching this far.

Today, the 18th of August 2022, I am on board a cruise ship headed to my home province in the Philippines for a short vacation. I just arrived in Manila last Friday after spending almost 3 years in Japan for my Ph.D. I thought 3 years were too short for Ph.D. research. But then it was a long time to miss home, especially my family and friends I haven't met for 3 years due to the pandemic.

Less than a month ago, I had my public research hearing. I still couldn't imagine that I can reach this far. That I will be writing this part of my manuscript intended to share my Ph.D. experiences and to express my sincerest gratitude to all the people who have been with me throughout this journey.

Most days I've spent were good days. But there were a lot of bad days, too, the days I've wished were just rainy days for shedding tears. It was definitely a humbling experience for me, knowing that I know less to nothing. That I have so much more to learn. I've failed so many times, felt lost along the way, and become unmotivated. But I've learned how to treat failures as an opportunity to grow, how to take one step backward so I can take two steps forward, and how to counter demotivation with discipline.

Throughout this journey, I am sincerely indebted to the following people who have supported, guided, mentored, challenged, and inspired me until today.

To my head supervisor Prof. Tsuyoshi Kawai, you have challenged me in a way I have never imagined before. Thank you for trusting and believing that I can always do better. To my co-supervisor Assoc. Prof. Yoshiyuki Nonoguchi, you have inspired me to continue working in this field. Thank you for all the support and guidance. Special thanks to the examination committee members Prof. Yukiharu Uraoka, Assoc. Prof. Tomoyuki Miyao, and Assoc. Prof. Naoaki Ono, for reading my manuscript and giving constructive comments during my midterm evaluation and public hearing. I would also like to thank Assoc. Prof. Takuya Nakashima, Asst. Prof. Mihoko Yamada, Asst. Prof. Marine Louis, Dr. Colin Martin, and Dr. Pablo Reine Diaz for all the help and guidance in the laboratory.

To all the members, past and present, of the Photonic and Reactive Molecular Science Laboratory, thank you for making my stay memorable - Dr. Junpei Kuno, Dr. Ryosuke

<div align="right">F.D. De los Reyes</div>